Mutations in genes encoding condensin complex proteins cause microcephaly through decatenation failure at mitosis

Mutations in genes encoding condensin complex proteins cause microcephaly through decatenation failure at mitosis

Carol-Anne Martin [1,13], Jennie E Murray[1,13], Paula Carroll[1], Andrea Leitch[1], Karen J Mackenzie[1], Mihail Halachev[1], Ahmed E Fetit[1], Charlotte Keith[2], Louise S Bicknell[1,3], Adeline Fluteau[1], Philippe Gautier[1], Emma A Hall[1], Shelagh Joss[4], Gabriela Soares[5], João Silva[6], Michael B Bober[7], Angela Duker[7], Carol A Wise[8], Alan J Quigley[9], Shubha R Phadke[10], The DDD study[11], Andrew J Wood[1], Paola Vagnarelli[12], Andrew P Jackson[1]

[1] MRC Human Genetics Unit, Institute of Genetics and Molecular Medicine, University of Edinburgh, UK

[2]South East Scotland Cytogenetics Service, Western General Hospital, Edinburgh, UK

[3] Department of Pathology, Dunedin School of Medicine, University of Otago, Dunedin, New Zealand

[4] West of Scotland Genetic Service, Southern General Hospital, Glasgow, UK

[5] Centro de Genética Médica Dr. Jacinto Magalhães, Centro Hospitalar do Porto, Porto, Portugal

[6]Instituto de Biologia Molecular e Celular (IBMC), Instituto de Investigação e Inovação em Saúde (I3S), Universidade do Porto, Porto, Portugal

[7] Division of Genetics, Department of Pediatrics, A.I. duPont Hospital for Children, Wilmington, Delaware, USA

[8] Sarah M. and Charles E. Seay Center for Musculoskeletal Research; Departments of Orthopedic Surgery, Pediatrics, McDermott Center for Human Growth and Development, University of Texas Southwestern Medical Center, Dallas, Texas 75350, USA

[9] Dept of Radiology, Royal Hospital for Sick Children, 9 Sciennes Rd, Edinburgh, UK

[10] Sanjay Gandhi Postgraduate Institute of Medical Sciences, Lucknow, India

[11] Wellcome Trust Sanger Institue, Hinxton, Cambridge, UK

[12] Biosciences, Research Institute for Health and Environment, Brunel University, London, UK

[13] These authors contributed equally to this work

Correspondence should be addressed to A.P.J. (andrew.jackson@igmm.ed.ac.uk)

Abstract

Compaction of chromosomes is essential for accurate segregation of the genome during mitosis. In vertebrates, two condensin complexes ensure timely chromosome condensation, sister chromatid disentanglement and maintenance of mitotic chromosome structure. Here, we report that biallelic mutations in *NCAPD2, NCAPH* or *NCAPD3*, encoding subunits of these complexes, cause microcephaly. As well, hypomorphic *Ncaph2* mice have significantly reduced brain size, with frequent anaphase chromatin bridge formation observed in apical neural progenitors during neurogenesis. Such DNA bridges also arise in condensin-deficient patient cells, where they are the consequence of failed sister chromatid disentanglement during chromosome compaction. This results in chromosome segregation errors leading to micronuclei formation and increased aneuploidy in daughter cells. These findings establish 'condensinopathies' as microcephalic disorders, with decatenation failure as an additional disease mechanism for microcephaly, implicating mitotic chromosome condensation as a key process ensuring mammalian cerebral cortex size.

Faithful and accurate segregation of the genome requires chromosome compaction and resolution of sister chromatids. At mitosis, chromosome condensation occurs through the large-scale reorganization of chromatin fibres and ensures the movement of chromosomes to daughter cells without DNA entanglement or entrapment by the cleavage furrow. In metazoans, mitotic chromosome assembly is mediated foremost through the activity of two protein complexes, condensin I and II (Hirano 2012). Condensin I and II complexes share the same overall arrangement with two core ATPases, SMC2 and SMC4 (structural maintenance of chromosomes), but differ in their three associated non-SMC subunits. In humans, the non-SMC subunits of condensin I are NCAPD2, NCAPG, and NCAPH (also known as Kleisin-γ), with the respective counterparts in the condensin II complex, NCAPD3, NCAPG2, and NCAPH2 (Kleisin-β) (Hirano and Mitchison 1994; Hirano et al. 1997).

Despite structural similarities, condensin I and condensin II have distinct functions with condensin II localized in the nucleus during interphase (Hirota et al. 2004) and required for early axial shortening of chromosomes in prophase (Shintomi and Hirano 2011). Cytoplasmic condensin I does not gain access to the chromosomes until after nuclear envelope breakdown (Hirota et al. 2004), when it contributes to the lateral compaction of metaphase chromosomes (Shintomi and Hirano 2011). In addition, condensins are required for the removal of catenations between replicated chromatids that arise during DNA

replication by facilitating topoisomerase II in actively resolving entangled sister chromatids (Baxter et al. 2011; Charbin et al. 2014).

In autosomal recessive primary microcephaly brain size is markedly reduced, resulting in a cranial volume comparable to that of human ancestors several million years ago (Woods et al. 2005). This condition has therefore been extensively studied to identify factors that regulate brain growth and neurogenesis. Similar reduction in cerebral cortex size is also seen in patients with microcephalic primordial dwarfism (MPD) where, unlike primary microcephaly, significant short stature is also evident (Klingseisen and Jackson 2011). The identification of disease genes common to both disorders (O'Driscoll et al. 2003; Bond et al. 2005; Al-Dosari et al. 2010; Kalay et al. 2011; Qvist et al. 2011; Martin et al. 2014) has established that primary microcephaly and MPD represent a phenotype spectrum in which a disproportionate reduction in brain volume relative to body size is seen (Verloes et al. 1993). Disease genes identified in these microcephalic disorders encode proteins integral to cell cycle progression (Klingseisen and Jackson 2011). Many encode centrosomal proteins essential for efficient mitotic spindle formation (Bond et al. 2002; Bond et al. 2005; Griffith et al. 2008; Nicholas et al. 2010) and consequently mutations result in perturbed cleavage plane orientation of neural progenitors (Fish et al. 2006; Gruber et al. 2011; Lancaster et al. 2013; Insolera et al. 2014). Therefore altered symmetric/asymmetric cell division dynamics in such neural stem cells has emerged as the major developmental mechanism for microcephaly (Thornton and Woods 2009). Here we report the identification of mutations in condensin complex genes, and demonstrate that these arise from a different mitotic mechanism, that establishes chromosome compaction and decatenation as critical processes ensuring normal mammalian brain growth.

Results

Mutations in condensin subunits cause microcephaly

To identify novel microcephaly genes, whole exome sequencing (WES) was performed on a cohort of patients with extreme microcephaly (OFC<-4 SD) due to reduced cerebral cortex volume with simplified gyri but without other structural abnormalities (Fig. 1A). In patient P1, a homozygous essential splice site mutation (c.4120+2T>C) in *NCAPD2* was detected, encoding one of the three non-SMC subunits of condensin I (Fig. 1B-D). In keeping with a pathogenic variant for a rare recessive disorder, it was present in a heterozygous state in both parents and was not reported in the ExAC database. To identify further mutations, we examined exome data from a further 94 families from our cohort. While no additional deleterious variants in *NCAPD2* were seen, in patient P2 compound heterozygous variants were observed in its paralog *NCAPD3* encoding the corresponding subunit in the condensin

II complex (Fig. 1E,F). These comprised, a frameshift mutation (c.1783_1784delG) and an intronic substitution (c.382+14A>G) predicted by *in silico* analysis (Alamut® Visual, Interactive Biosoftware) to create a new splice donor site within intron 3.

Having identified mutations in subunits of condensin I and II, we therefore proceeded to screen all eight genes that encode proteins in these two complexes using a custom Ampliseq multiplex PCR panel and Ion-Proton™ semiconductor sequencer. Sequencing of 198 patients with microcephaly phenotypes ranging from primary microcephaly to microcephalic dwarfism, identified a third patient (P3, OFC -4.2 s.d., Fig. 1A, Supplemental Table S1) with a homozygous missense variant in *NCAPH* (c.728C>T, p.Pro243Leu), encoding the kleisin subunit of the condensin I complex. This substitution was at an evolutionary conserved residue (Fig. 1G, conserved to *Saccharomyces cerevisiae*) and was predicted to have a deleterious effect by *in silico* analysis (Polyphen-2, Mutation Taster, Mutation Assessor). We then extended our search to the DDD study (Deciphering Developmental Disorders 2015), representing a wide range of developmental disorders (n=1,000 exomes). This identified a fourth microcephalic patient (P4, OFC -2.7 s.d., Supplemental Table S1) with a homozygous missense mutation in the condensin II gene *NCAPD3* (c.3458T>G, p.Glu1153Ala), resulting in a deleterious amino acid substitution at a residue highly conserved in condensin II orthologues (Fig. 1H). All variants identified were confirmed by capillary sequencing and all parents established to be heterozygous carriers consistent with autosomal recessive inheritance (Table 1). None of the variants were reported in the large-scale control dataset ExAC.

Severity of microcephaly correlated with mutation type, ranging from -2.7 to -11.9 s.d. (Supplemental Table S1, Supplemental Fig. S1A), and was most severe in P1 and P2 in which frameshift/splice-disrupting variants were found. Missense mutations in P3 & P4 were accompanied by milder microcephaly. Though less severely affected, stature was also significantly reduced in P1 and P2, with height within normal population limits in P3 and P4. No distinctive facial features or associated malformations were apparent (Supplemental Fig. S1B) and, apart from intellectual disability, co-morbidity was limited except for P2 who died of a malignant anaplastic medulloblastoma at 11 yrs (Fig. 1A, Supplemental Table S1).

Condensin mutations impair chromosome structural integrity

To confirm the pathogenic nature of the identified mutations, we established primary fibroblast lines from all four patients and assessed the effect of these mutations on transcript splicing and protein expression by RT-PCR and immunoblotting respectively. The nucleotide substitution c.4120+2T>C in *NCAPD2* abolished the exon 31 consensus splice donor site and RT-PCR demonstrated that this resulted in retention of intron 30, with residual wild-type

transcript only just detectable (Fig. 2A). The incorporation of intron 30 was confirmed by capillary sequencing (data not shown), and results in a transcript encoding an additional 29 amino acids before a premature termination codon that led to omission of the most C-terminal 28 amino acids encoded by exon 31. Furthermore, a significant reduction in NCAPD2 protein was seen in patient primary fibroblasts (Fig. 2B, Supplemental Fig. S2A, p=0.0086), presumably resulting from decreased stability of the mutated protein (given the C-terminal location of the mutation, nonsense-mediated decay (NMD) is not expected).

Heterozygous 1783_1784delG and 382+14A>G variants in *NCAPD3* were predicted to introduce premature termination codons (PTC) after exon 3 and in exon 15 respectively leading to NMD of the resulting transcripts. Consistent with this, substantially reduced wild-type *NCAPD3* transcript levels were seen in P2 fibroblasts (Fig. 2C). A transcript resulting from the alternative donor splice site generated by the c.382+14A>G substitution was not detected. However, an additional transcript was observed which deleted exon 3, likely arising from nonsense associated altered splicing (Wang et al. 2002). This transcript was consequently out of frame, resulting in premature termination (p.Ser74Alafs*3). A low level of normally spliced transcript was detectable that likely accounts for the low levels of residual NCAPD3 protein observed on immunoblotting (Fig. 2D and Supplemental Fig. S2B). We therefore concluded that mutations in both P1 and P2 led to substantial effects on transcript and proteins of the affected condensin subunits. However, we expect these to result in significant loss of function rather than being functionally null, given the essential nature of condensins in vertebrates (Hudson et al. 2003; Smith et al. 2004; Nishide and Hirano 2014; Houlard et al. 2015). In contrast, amino acid substitutions in P3 and P4, in *NCAPH* (p.Pro243Leu) (Supplemental Fig. S2C,D) and *NCAPD3* (p.Glu1153Ala) (Fig. 2D) respectively, did not affect cellular protein levels. Although outside annotated domains, the substitutions are at highly conserved residues (Fig. 1G,H) and so are likely to affect condensin complex function.

As both condensin I and II have established roles in ensuring axial and radial stability of compacted chromatin (Hudson et al. 2003; Ono et al. 2003; Hirota et al. 2004; Green et al. 2012), we next assessed the impact of P1-P4 patient mutations on condensin function in mitotic chromosome integrity. We utilised an established intrinsic chromosome structure assay (ICS) (Fig. 2E) that has been previously used to demonstrate structural integrity defects in *SMC2*, *NCAPH* and *NCAPD3* conditionally null DT40 cells (Hudson et al. 2003; Green et al. 2012). This is a qualitative assay that assesses whether chromosomes are able to recover higher-order structure after unfolding chromatin in low-salt TEEN buffer (which increases DNA-DNA repulsion through cation-depletion). In this *in vitro* assay, mitotic chromosomes from all patient cell lines failed to efficiently recover their normal condensed

appearance after two rounds of unfolding/refolding in marked contrast to two control primary fibroblast cell lines (C1=1.7+/-0.7%, C2=3.2+/-0.6%, P1=34.6+/-0.6%, p<0.0001, P2=41.6 +/-5.7%, p=0.0026 P3=77.7+/-3.5%, p<0.0001, P4=49.4 +/-6.3%, p=0.0019) (Fig. 2F,G). Morphologically, structurally disrupted patient chromosomes resembled those previously reported in DT40 cells lacking *NCAPH* and *NCAPD3* (Green et al. 2012) (Fig. 2G). We therefore concluded that mutations in all 4 patients can disrupt condensin dependent mitotic chromosome integrity, providing functional supporting evidence for their pathogenicity.

Chromatin bridges in Ncaph2 apical neural progenitors lead to microcephaly

To extend our investigations into a developmental system we next examined a published hypomorphic loss of function *Ncaph2* condensin II mouse mutant[42] with a single missense mutation (p.Ile15Asn), in which brain size and neurodevelopment had not been previously assessed. Measurement of brain size at 8 weeks postnatally demonstrated significantly reduced brain weight (*Ncaph2*$^{I15N/+}$ *z*=0.06+/-0.2*, Ncaph2*$^{I15N/I15N}$*z*= -0.6+/-0.15, p=0.01) and reduced cortical surface area (*Ncaph2*$^{I15N/+}$ *z*=0.08+/-0.26*, Ncaph2*$^{I15N/I15N}$*z*= -1.4+/-0.16, p=0.0001), in comparison to *Ncaph2*$^{I15N/+}$ littermate controls (Fig. 3A, B, Supplemental Fig. S3A). Reduced body weight was also evident in *Ncaph2*$^{I15N/I15N}$ mice (*Ncaph2*$^{I15N/+}$ *z*=0.12+/-0.23*, Ncaph2*$^{I15N/I15N}$ *z*= -1.45+/-0.3, p=0.0003, Supplemental Fig. S3B). Having confirmed that mutation of a non-SMC condensin subunit also caused microcephaly in mice, we then investigated how neurogenesis was perturbed during embryonic development. In the E13.5 *Ncaph2*$^{I15N/I15N}$ embryonic brain, a 4 +/-1.6% reduction in neocortical thickness was seen, while the relative thickness of ventricular/subventricular zones (VZ/SVZ, PAX6 positive cells, *Ncaph2*$^{I15N/+}$ =76.5 +/-0.7%, *Ncaph2*$^{I15N/I15N}$ =78 +/-0.4%, p=0.12) and the neuronal preplate (PP) layer (Tub βIII positive*, Ncaph2*$^{I15N/+}$ =22.4 +/-0.4%, *Ncaph2*$^{I15N/I15N}$ =22.3 +/-0.4%, p=0.83) was unchanged (Fig. 3C,D).

We also measured mitotic spindle orientation of apical progenitors that has previously been found to be perturbed in microcephaly models (Lizarraga et al. 2010; Gruber et al. 2011; Lancaster et al. 2013). As 2-dimensional analysis of spindle axis can lead to systematic measurement errors (Juschke et al. 2014), metaphase and anaphase apical progenitors were imaged by spinning-disc confocal and axis orientation was determined in 3-dimensions.The angle between the line bisecting both spindle poles (mitotic centrosomal marker, Aurora A), and the plane of the ventricular surface was measured in E13.5 brain sections (Fig. 3E,F and Supplemental Fig. S4A,B), demonstrating that the mitotic spindle position in *Ncaph2*$^{I15N/I15N}$ neuroepithelia was indistinguishable from controls (Fig. 3G, Supplemental Fig. S4C) (30-60° bin, *Ncaph2*$^{I15N/+}$ =7 +/- 1.4%, *Ncaph2*$^{I15N/I15N}$=10.8 +/- 5.9%, p=0.57; 60-90° bin, *Ncaph2*$^{I15N/+}$ =0.8 +/- 0.8%, *Ncaph2*$^{I15N/I15N}$=0.6 +/- 0.6%, p=0.83). This

therefore indicated that a different process underlies condensin-associated microcephaly, and upon further characterisation we observed frequent chromatin bridges during anaphase in *Ncaph2*$^{I15N/I15N}$ apical progenitors (Fig. 3H-J). Such bridges were at a significantly higher frequency than heterozygous controls (Fig. 3J, *Ncaph2*$^{I15N/I15N}$=39.5 +/- 5.5%, *Ncaph2*$^{I15N/+}$ =18.4 +/- 2.4%, p=0.02). As DNA bridges are known to lead to chromosome segregation errors, and impaired cell survival, this provided an alternative explanation for condensin microcephaly (model, Fig. 3K). To investigate this mechanism in more detail we next employed a cell biological approach, utilizing the patient and mouse cell lines available to us.

Decatenation failure leads to DNA bridges in condensin-deficient cells

Firstly, to characterize the cause of such DNA bridges, we examined mitosis in condensin-deficient patient cells. Analysis of P1 and P2 fibroblasts, representing mutations in condensin I and II respectively, both demonstrated DNA bridges, confirming such mitotic abnormalities also occurred in condensin microcephaly patients. In P2 (*NCAPD3*) fibroblasts elevated levels of chromatin bridges and lagging chromatin/chromosomes were observed during mitosis, evident in 16.7% of anaphases (C1=3.1 +/-1%, P2=16.7+/-2.6%, p=0.003) (Fig. 4A,C). Such chromosome segregation errors have been previously reported in NCAPD3 deficient cells (Ono et al. 2004; Gerlich et al. 2006) but consistent with P2 patient cells retaining residual condensin II function we observed this occurred to a lesser extent than in conditionally null *NCAPD3* DT40 cells, in which 80% of anaphase and telophase cells had prominent chromatin bridges (Green et al. 2012). A similar level of segregation defects to that present in patient P2 was also seen in *Ncaph2*$^{I15N/I15}$ MEFs, significantly higher than heterozygote littermate-derived control lines (*Ncaph2*$^{I15N/+}$ #1=6.3+/-0.7%, *Ncaph2*$^{I15N/I15N}$#1=17.9% +/- 1.7%, p=0.0013, *Ncaph2*$^{I15N/I15N}$#2=13 +/- 0.4%, p=0.0001) (Supplemental Fig. S5A).

In P1 cells, a significantly increased frequency of substantial DNA bridges was not evident on DAPI staining. However finer chromatin bridges have been observed in condensin I deficient cells (Green et al. 2012) and loss of both condensin complexes has previously been shown to increase the number of ultra-fine DNA bridges (UFBs) (Lukas et al. 2011). To sensitively detect UFBs we performed PICH (PLK1 interacting checkpoint helicase) immunostaining and using this methodology we observed a substantial increase in persisting UFBs in both condensin I and condensin II cells in mid to late anaphase (C1=19.4+/-2.4%, P1=44.1+/-5.6%, p=0.02, P2=33.5+/-3.3%, p=0.04) (Fig. 4B,C).

We next considered the origin of the observed DNA bridges. UFBs are believed to originate either from unresolved sister chromatid entanglements as double-stranded DNA catenanes (Chan et al. 2007) or at regions of incomplete DNA replication termed late-

replication intermediates 'LRIs' (Chan et al. 2009). The latter can be induced by replication stress and is associated with paired FANCD2 foci which flank LRI UFBs. Such sister FANCD2 foci were not evident in P1 and P2 patient cells (Fig. 4D), indicating that observed UFBs were more likely due to dsDNA catenenes. Furthermore, UFBs, chromatin bridges and lagging chromosomes/chromatin identical to those observed in patient cells were also observed in control fibroblasts in which cellular decatenation activity was inhibited by treatment with low levels of the topisomerase IIα inhibitor ICRF159 (Fig. 4E).

Micronuclei and aneuploidy are consequences of impaired chromosome segregation

To establish how reduced cellularity arises in condensin patients, we examined the post mitotic consequences of decatenation failure by live-imaging of patient fibroblasts transiently expressing RFP-H2B (Fig. 5A). This confirmed a significant increase of anaphase cells with chromatin bridges in P2 fibroblasts, consistent with the previous analysis of fixed patient cells (Supplemental Fig. S5C; C1= 6.1%, C2=2.4%, P2= 14.6%, p=0.0056). Furthermore, some of the chromatin bridges were seen to lead to micronuclei formation at later time points (Fig. 5A). Analysis of fixed DAPI-stained interphase cells confirmed increased levels of such micronuclei in both P1 and P2 fibroblast lines (C1=0.7 +/-0.2%, P1=2.9+/-0.6%, p=0.009, P2=5.4 +/-0.6%, p=0.0001) (Fig. 5B). In P3 and P4, microcephaly without significant short stature was observed. In keeping with this milder clinical phenotype restricted to the CNS, increased micronuclei formation was less pronounced in P3 fibroblasts, and was not detected in P4 fibroblasts (P3=1.3+/-0.3%; 0.4+/- 0.2% p=ns). An *in vivo* erythrocyte micronuclei assay demonstrated that micronucleated cells were significantly more frequent in homozygous mutant mice compared to wild type control animals (*Ncaph2*$^{I15N/I15N}$ reticulocytes =0.168% +/- 0.01%, p=0.005, *Ncaph2*$^{I15N/I15N}$ mature erythrocytes=1.5 +/- 0.04%, p=0.01) (Fig. 5C). Interphase FISH with chromosome specific alpha-satellite probes (Fig. 5D) demonstrated a significant increase of P1 and P2 primary fibroblast cells with altered numbers of centromere signals compared with controls, consistent with a low level of increased aneuploidy in both cell lines (C1=7.8+/-0.7%, P1=10.7+/- 0.3%, p=0.03, P2=13.8+/- 0.2%, p=0.0006). Taken together, we concluded from these cellular experiments that decatentation failure leads to the formation of micronuclei and aneuploidy in condensin-deficient patient cells.

Discussion

Human germline mutations in condensin protein subunits

Here we report that mutations in genes encoding subunits of condensins cause microcephaly, establishing that disrupted chromosome condensation can result in reduced brain size. This provides a further example of where aggregate analysis of genes encoding macromolecular complexes has permitted identification of rare human disease genes (Crow et al. 2006; Bicknell et al. 2011; Mannini et al. 2013). Using a similar strategy, somatic mutations in condensins have also been associated with several cancer types (Leiserson et al. 2015). This and the fatal brain tumour in patient P2, raises the possibility that germline condensin mutations are also cancer pre-disposing.

Consistent with the cell-essential nature of condensins due to their requirement for cell division (Strunnikov et al. 1995; Hagstrom et al. 2002; Hudson et al. 2003; Ono et al. 2003; Oliveira et al. 2005; Siddiqui et al. 2006), the patient mutations reported here are all functionally hypomorphic. The implicit developmental viability of these human mutations therefore has utility for providing further insights into the roles of these essential protein complexes at the organism level.

Both condensin I and II are required to resolve UFBs formed by dsDNA catenanes

In addition to identifying three new human disease genes, we establish decatenation failure as a novel pathogenic mechanism for microcephaly, mitotic in origin and distinct from mechanisms associated with previously identified disease genes (model, Fig. 3K). This contrasts with the disrupted transcriptional regulation that underlies ‘cohesinopathies’ (Dorsett 2011), which result from mutations in the paralogous cohesin complex (Musio et al. 2006; Deardorff et al. 2007; Deardorff et al. 2012). The identification of mutations in both condensin I and II complexes supports a mitotic basis, as both are required for mitotic chromosome integrity (Hudson et al. 2003; Ono et al. 2003; Hirota et al. 2004) and only colocalise at mitosis on compacting chromatin (Hirota et al. 2004). Furthermore, mitotic chromosome integrity is impaired in patient cell lines irrespective of which condensin is affected.

Our results indicate that decatenation failure is likely the direct consequence of such impaired chromosome compaction. Substantial chromatin bridging has been described in condensin II null cells and finer DAPI positive bridges occur in condensin I knockout cells (Green et al. 2012). While condensin II patient cells have similar macroscopic chromatin bridges, albeit at lower rates than previously reported, such chromatin bridges were not

increased in condensin I cells. This led us to assess if DNA bridges not visualised by DAPI might be present. PICH immunostaining permitted the detection of ultrafine bridges (UFBs) that have not previously been reported in cells deficient for either condensin I or condensin II. Such single non-chromatinised DNA fibres point to failed decatenation as the origin of the bridges (Baumann et al. 2007; Chan et al. 2007; Ke et al. 2011), rather than these arising directly from disordered chromosome structure. Mechanistic studies in yeast have demonstrated that condensins promote decatenation (D'Ambrosio et al. 2008; Baxter et al. 2011; Charbin et al. 2014) and it has been proposed that condensin-mediated chromosome compaction increases tension in catenated DNA that remains between sister chromatids, such that it provides directionality to topoisomerase II mediated strand exchanges towards chromatid decatenation (Model, Fig. 5E) (Cuylen and Haering 2011).

Studies of replication stress associated UFBs at fragile sites have implicated condensins in promoting their resolution (Minocherhomji et al. 2015). However rather than solely dealing with 'late replicating intermediate' (LRI) UFBs, we establish here that both condensin complexes are also required to resolve double-stranded DNA catenanes that occur in unperturbed cells, as UFBs were not flanked by FANCD2, a marker of LRI UFBs. Additionally, we observe a differential requirement for condensin I and II in UFB resolution, with condensin II specifically needed for decatenation of centromeric UFBs (Supplemental Fig. S5B), while condensin I UFBs arise at distributed sites that are not predominantly centromeric or ribosomal DNA (data not shown). Such differences could be accounted for by differing localisation on mitotic chromosomes (Ono et al. 2003; Ono et al. 2004), and/or their differential roles in axial and lateral chromosome compaction (Shintomi and Hirano 2011). Therefore, the study of hypomorphic mammalian cell lines establishes that both condensins act in the resolution of dsDNA catenanes, suppressing UFB formation during unperturbed cell cycle.

Decatenation failure as a cause of microcephaly

The model currently favoured for the majority of primary microcephaly genes is that altered mitotic spindle position leads to an altered cleavage plane at cytokinesis, and consequently perturbed symmetric/asymmetric fate decisions (Fig. 3K). In contrast to centrosomal models of microcephaly, spindle orientation is not altered in condensin-deficient apical progenitors (neural stem cells). Furthermore, normal proportions of PAX6 progenitors and TUJ1-positive neurons are maintained in the developing neuroepithelium, consistent with unperturbed symmetric/asymmetric cell fate choice. Therefore, while microcephaly associated with condensin mutations has a mitotic origin, it arises by a different mechanism that originates from DNA bridges in dividing apical neural progenitor cells as a result of decatenation failure.

Macroscopic chromatin bridges are an established cause of chromosome segregation failure (Hoffelder et al. 2004). Consistent with this, we observed lagging chromosome fragments by live imaging in condensin II patient cells and consequently micronuclei in the subsequent interphase. Micronuclei also arose in condensin I patient cells, suggesting that UFBs may also prevent timely chromosome segregation, a conclusion supported by findings in PICH knockout DT40 cells (Nielsen et al. 2015). Therefore despite the differing mitotic roles of the two condensin complexes, missegregation of chromatin likely explains the shared phenotype and disease presentation. Furthermore, the high frequency of UFBs in Blooms syndrome (Chan et al. 2007) would also predict that microcephaly in this disorder occurs by the same mechanism.

Notably the protein encoded by the previously identified primary microcephaly gene *MCPH1* is a regulator of chromosome condensation that inhibits condensin II (Trimborn et al. 2006; Yamashita et al. 2011) and interacts with both NCAPD3 and NCAPG2 subunits (Wood et al. 2008; Yamashita et al. 2011). This raises the possibility that similar mechanisms could contribute to reduced brain size in MCPH1 patients. However MCPH1 has also been reported to function in centrosomal Chk1-dependent checkpoint signalling (Tibelius et al. 2009) that when impaired in *Mcph1*$^{-/-}$ mice results in altered mitotic spindle orientation and increased asymmetric cell division in neural stem cells (Gruber et al. 2011). Nonetheless, given that mutations in condensins are now also found to cause microcephaly, further investigation of the MCPH1-condensin interaction is warranted.

We observed that chromosome segregation failure leads to aneuploidy in patient cells, itself an established cause of microcephaly (Hanks et al. 2004; Marthiens et al. 2013). Aneuploidy has been shown to impair proliferation potential and cell survival, with CIN models in yeast and mammals establishing that chromosome segregation failure leads to cell cycle delay and/or arrest (Santaguida and Amon 2015), processes that would act to reduce neuronal cell number during the rapid cell proliferation of neurogenesis. DNA damage is also likely to occur at persisting chromatin bridges (Janssen et al. 2011; Maciejowski et al. 2015) and in micronuclei (Crasta et al. 2012), which may well impair cell viability, increasing the already high levels of apoptosis that occurs during brain development. Diminished cell survival would also result in reduced brain size, and is consistent with the increased cell death seen in Nestin-cre condensin I and II knockouts (Nishide and Hirano 2014). Therefore, we propose that impaired decatenation with subsequent chromosome segregation failure results in reduced cell proliferation and increasing cell death, providing a straightforward explanation for microcephaly associated with hypomorphic condensin mutations. While the restricted developmental window for

neurogenesis provides one explanation for the disproportionate effect on brain size, there is also an elevated number of chromatin bridges in condensin deficient neural stem cells (Fig. 3J, S5A (Nishide and Hirano 2014)) that could also explain why this organ is more severely affected.

In summary, through the identification of mutations in multiple condensin subunits we show that ‘condensinopathies’ result in microcephaly due to impaired DNA decatenation, establishing this as a novel disease mechanism and chromosome compaction as a key process ensuring mammalian cortical size.

Methods

Research subjects

Genomic DNA from the affected individuals and family members was extracted from peripheral blood by standard methods or obtained from saliva samples using Oragene collection kits according to manufacturer's instructions. Informed consent was obtained from all participating families and the studies were approved by the ethics review board at the Scottish Multicentre Research Ethics Committee (04:MRE00/19) and the University of Texas Southwestern Medical Center (STU112010-149). Parents provided written consent for the publication of photographs of the patients. For growth measurements, z-scores (standard deviations from population mean for age and sex) were calculated using LMSgrowth based on British 1990 growth reference data (Freeman et al. 1995).

Animal studies

All mouse studies were conducted under guidance and approval issued by the Medical Research Council in Responsibility in the Use of Animals for Medical Research (July 1993) and Home Office Project Licence. The *Ncaph2*$^{I15N/I15N}$ mouse was identified from an ENU screen as having an unusual, isolated T lymphocyte developmental defect that altered circulating T cell number with increased levels of the activation/memory marker CD44, but which was reported as otherwise healthy, fertile and without other phenotypes (Gosling et al. 2007). The *Ncaph2*$^{I15N/I15N}$ mouse line was maintained on a C57BL6/J background.

Exome sequencing, AmpliSeq resequencing, and Sanger sequencing.

Exome sequencing and variant filtering performed as described previously (Martin et al. 2014; Murray et al. 2015) for patient P1 and P2. Exome sequencing for patient P4 (DDDP261277) was performed by the DDD study as described (Wright et al. 2014). Ion AmpliSeq multiplex PCR (Life Technologies) was used for cohort NGS resequencing as described previously (Murray et al. 2015). Briefly, primers were designed to amplify coding exons of all condensin I and II genes with 25 bp of flanking intronic sequence. PCR amplification performed in 1/6th reaction volumes for primer pools using 5 ng of patient DNA. After pooling patient amplicons, Ion Xpress barcoding was performed and sequenced on the Ion Proton sequencing platform (Life Technologies) using Ion P1 200 Sequencing Kit. Variant calling, Torrent Suite software; filtering as for exome analysis. All variants were confirmed by capillary sequencing of PCR products amplified from the relevant condensin gene (primer sequences in Supplemental Table S2A), on an ABI 3730 capillary sequencer. Sequence traces were analyzed using Mutation Surveyor software (SoftGenetics Inc.).

Sequence alignment and secondary structure prediction

Sequences were obtained from Ensembl release 78 and Ensembl Genomes Release 25 (except for Chlamydomonas: from Phytozome 10.3)**.** Protein sequences were aligned using clustalw (CLUSTAL 2.1). As not all eukaryotes have condensin II complexes, homologs were selected from species listed in Fig.1 as described in (Hirano 2012). Amino acid similarity was scored using Blossom 45. The location of NCAPH domains were determined based on the above alignment and secondary structure predictions made by the JPRED server.

RT-PCR

Total RNA was isolated from human primary fibroblast cell lines using the RNeasy kit (Qiagen) according to manufacturer's instructions. After DNAse I treatment (Qiagen), cDNA was generated using random oligomer primers and AMV RT (Roche). RT-PCR primers, Supplemental Table S2B.

Cell culture

Dermal fibroblasts were obtained by skin punch biopsy and cultured in amnioMAX C-100 complete medium (Life Technologies). Mouse embryonic fibroblasts were prepared from individual E13.5 embryos after removing the head and abdominal cavities. Each embryo was minced and maintained in DMEM, 10% FCS, 0.1 mM β-mercaptoethanol, 100 U/ml penicillin and 100 µg/ml streptomycin. All fibroblast cultures were maintained in a 37°C incubator with 5% CO_2 and 3% O_2. hTERT RPE-1 cells were obtained from the American Type Culture Collection (CRL-4000) and cultured in DMEM:F12, 10% FCS, 0.26% sodium bicarbonate, 100 U/ml penicillin and 100 µg/ml streptomycin. All cell lines were routinely tested for mycoplasma. Short interfering RNA (siRNA) oligonucleotides were transfected into hTERT RPE1 cells using RNAi MAX (Life Technologies) according to manufacturer's instructions. SiRNA oligonucleotide sequences, Supplemental Table S2C. pRFP-H2B was transfected into primary fibroblast cells by electroporation with the Neon transfection system (Thermo Fischer Scientific) according to manufacturers' instructions. Where indicated, cells were treated with 0.3µM aphidicolin (Sigma Aldrich) or 5µM ICRF-159 (Sigma Aldrich) for 24 h.

Flow cytometry

Peripheral blood micronuclei assays were performed using ~50 µl blood collected into 200 µl heparin solution. 180 µl of this mixture was pipetted into 2 ml methanol, which had been pre-chilled at -80^{o}C for 24 h. Samples were stored at -80°C for at least 24 h, washed in PBS and resuspended in 50 µl of

PBS. 20 µl was transferred to a new tube containing 69 µl PBS, 1 µl ant-CD71 antibody (RI7217 Biolegend) and 10 µl of RNAse A solution (10 mg/ml) and incubated for 1 h on ice. 500 µl of PBS containing 1.25 µg/ml propidium iodide solution was added immediately prior to analysis. FACS data was acquired on a BD FACSAria II cell sorter and processed using FlowJo software (Treestar).

Chromosome analysis

Metaphases and nuclei were isolated in hypotonic buffer (0.25% KCl, 1% $Na_3C_6H_5O_7$), then fixed with methanol:acetic acid (3:1) and dropped onto slides. Metaphase chromosomes were visualised with DAPI staining. Interphase FISH utilised chromosome enumeration probes labelled in Spectrum orange/green/aqua (Abbot Molecular) prepared in CEP hybridization buffer (Abbot Molecular). Slides were scanned on the GSL-120 Automated Slide Scanner and analysed using Cytovision version 7.3.1 (Leica Biosystems).

Intrinsic chromosome structure assay

Primary fibroblasts were grown on poly-L-lysine (Sigma-Aldrich) coated coverslips and blocked with 200 ng/µl nocodazole overnight. Cells were incubated in 75mM KCl buffer for 5 min followed by TEEN buffer (0.5 mM triethanolamine-HCl [pH 8.5], 0.1 mM Na EDTA, 12.5 mM NaCl) for 30 min and RSB (10 mMTris-HCl [pH 7.4], 210 mM NaCl, and 5 mM $MgCl_2$) for 10 min. The TEEN-RSB cycle was then repeated, cells were fixed in Methanol:Acetic Acid (3:1) for 30 min and coverslips mounted in DAPI.

Immunofluorescence and microscopy

Human dermal fibroblasts and mouse embryonic fibroblasts were grown on untreated coverslips (Becton Dickinson). Cells were fixed in 4% PFA (TAAB) in PHEM (25 mM Hepes-NaOH [pH 6.8], 100 mM EGTA, 60 mM PIPES, 2 mM $MgCl_2$) for 15 min. Following PFA fixation, cells were permeabilised by treatment in 0.2% Triton-X-100 in PHEM for 2 min. Fixed cells were blocked in PBS/1% bovine serum albumin (Sigma-Aldrich), incubated with anti-PICH antibody (Ke et al. 2011) or FANCD2 (Santa cruz, sc-20022) for 30 min, followed by anti-rabbit IgG Alexa Fluor 568 linked (Life Technologies A11036) or anti-mouse IgG Alexa Fluor 488 linked (Life Technologies A11029) and DAPI. For UFB scoring, mid to late anaphase cells were selected on the criteria that tips of segregating sister chromatids were between 12-20 µm apart and that no nuclear envelope reformation was visible. Epifluorescent images were acquired using a Imager A1 fluorescence microscope (Zeiss) controlling a Photometrics Coolsnap HQ2 CCD camera and a piezoelectrically driven objective mount was used to control movement in the z dimension. Images were captured using a 100 X Plan-APOCHROMAT (1.4 NA) objective at 0.2 µm z-sections and subsequently deconvolved using Volocity software

(PerkinElmer). For live imaging, primary fibroblast cells were seeded onto glass bottom plates (Greiner Bio One) and imaging acquired in a closed chamber system with Leibovitz L-15 medium (Gibco). TRITC image data sets were collected with a Axiovert 200 fluorescence microscope system (Zeiss) heated to 37°C equipped with a 40 X PLAN NEOFLUOR (0.75NA) objective. Image capture was performed using metamorph (Molecular Devices). Images with Z optical spacing of 2 µm were recorded every 10 min for a 24 h period.

Western blotting

Cells were lysed in 50 mMTris-HCl [pH8], 280 mM NaCl, 0.5% NP40, 0.2 mM EDTA, 0.2 mM EGTA and 10% glycerol supplemented with protease inhibitor tablet (Roche). Protein samples were run on a 4-12% NuPAGE Bis-Tris precast gel (Life Technologies) followed by immunoblotting using anti-NCAPD3 (Bethyl Laboratories A300-604A), NCAPD2 (Bethyl Laboratories A300-601A), NCAPH (Bethyl Laboratories A300-603A) and anti-actin (Sigma A2066).

Mouse genotyping, immunofluorescence and microscopy

For mouse genotyping, ear-clips were boiled in 50 µl (25 mM NaOH, 0.2 mM EDTA) for 30 min at 95°C, cooled, then neutralized with 50 µl 40 mM Tris base and used directly in PCR reactions. For genotyping of embryos, tails were treated with DirectPCR Lysis Reagent (Viagen) according to the manufacturer's instructions. All genotyping PCRs were performed using the primer pair in Table S2D and digested by *BccI* prior to electrophoresis.

E13.5 embryos and postnatal mice (P50-58) were dissected in ice-cold PBS. The E13.5 embryos were fixed for 5 h in 4% paraformaldehyde/PBS and postnatal mouse brains were dissected and fixed overnight in 4% formaldehyde/PBS. For cryosectioning, the samples were cryoprotected through a sucrose/PBS series (5%, 10%, 15% and 20%), embedded in O.C.T. compound (Cellpath) and stored at –80°C. All cryostat sections were cut at 12 µm. Immunofluorescence staining was performed by permeabilizing with 0.2% Triton X-100/PBS for 15 min, blocking in 1% BSA/PBS and primary incubation overnight. Primary antibodies used were anti-TUBβIII (Covance MMS-435P), PAX6 (Covance PRB-178P) and Aurora A (BD transduction Labs 610939). Secondary antibodies were incubated for 2 hr and all immunofluorescence was co-stained with DAPI. Imaging was performed using dragonfly multimodal imaging platform in 3D fast confocal mode using the 405, 488 and 561nm lasers and a iXon Ultra 888 EMCCD Camera (Andor). Images were captured using a 100 X Plan-APOCHROMAT (1.4 NA) or 60 X Plan-APOCHROMAT (1.4 NA) objective at 0.2 µm z-sections.

3D measurements of spindle orientations

Analysis was restricted to cells in metaphase and anaphase as the mitotic spindle stops rotating along the apico-basal axis from metaphase onwards (Haydar et al. 2003). Two assumptions were made to measure mitotic spindle orientations in three-dimensions. Firstly, the spindle axis was defined by a straight line through two points defined by the xyz coordinates of the two centrosomes (Aurora A signal). Secondly, the ventricular surface was defined using three points to establish a three-dimensional plane. These points were manually annotated for each 3D image using the OMERO (5.1.4). Mitotic spindle orientation was calculated using a custom-written GUI software developed using MATLAB (R2015a). This calculated the normal vector to the plane representing the ventricular surface, and then the cosine angle, 'A', between this normal vector and the spindle line vector. The mitotic spindle orientation angle was thus, 90^{o}-A (ie. the complementary acute angle). Z-axes calibrations were accounted for when defining the points' spatial locations. 3D reconstructions were rendered using Imaris software (Andor).

Statistical analysis

All data are shown as averages, with variance either as s.e.m or s.d. Statistical analysis was performed using Prism (Graphpad Software Inc.). For all quantitative measurements, normal distribution was assumed, with t-tests performed, unpaired and two-sided unless otherwise stated. For categorical data, X^2-test was used. Data collection and analysis were not performed blind, as the different conditions were clearly recognizable by the experimenter. No statistical methods were used to predetermine sample sizes, which were determined empirically from previous experimental experience with similar assays, and/or from sizes generally employed in the field.

URLs.

http://exac.broadinstitute.org; http://phytozome.jgi.doe.gov/pz/portal.html;

http://www.compbio.dundee.ac.uk/jpred4

Acknowledgements

We thank the families, J.Tolmie and other clinicians for their involvement and participation; Potentials Foundation and Walking with Giants Foundation; W. Bickmore, M. Reijns for comments on the manuscript; J. Marsh, C. Ponting, Matt Hurles, Phil Jones and E.Hall for helpful discussions; H. Yu (Howard Hughes Medical Institute) for his kind gift of the PICH antibody; E. Freyer for assistance with FACS analysis; D. Read for technical assistance; the IGMM core sequencing service and IGMM imaging facilities; WGH Biological Research Facility staff for animal husbandry, OGT and Edinburgh CRF for NGS sequencing. This work was supported by funding from the MRC, the Lister Institute for Preventative Medicine and the European Research Council (ERC, 281847) (A.P.J.), BBSRC grant (BB/K017632/1)(P.V), a Sir Henry Dale Fellowship (Grant 102560/Z/13/Z)(A.J.W.), Medical Research Scotland (L.S.B.), the Potentials Foundation (C.A.W.), Indian Council of Medical Research (BMS 54/2/2013)(S.R.P). The DDD study presents independent research commissioned by the Health Innovation Challenge Fund [grant number HICF-1009-003], a parallel funding partnership between the Wellcome Trust and the Department of Health, and the Wellcome Trust Sanger Institute [grant number WT098051]. The views expressed in this publication are those of the author(s) and not necessarily those of the Wellcome Trust or the Department of Health. The study has UK Research Ethics Committee approval (10/H0305/83), granted by the Cambridge South REC, and GEN/284/12 granted by the Republic of Ireland REC). The research team acknowledges the support of the National Institute for Health Research, through the Comprehensive Clinical Research Network.

Martin_Fig1

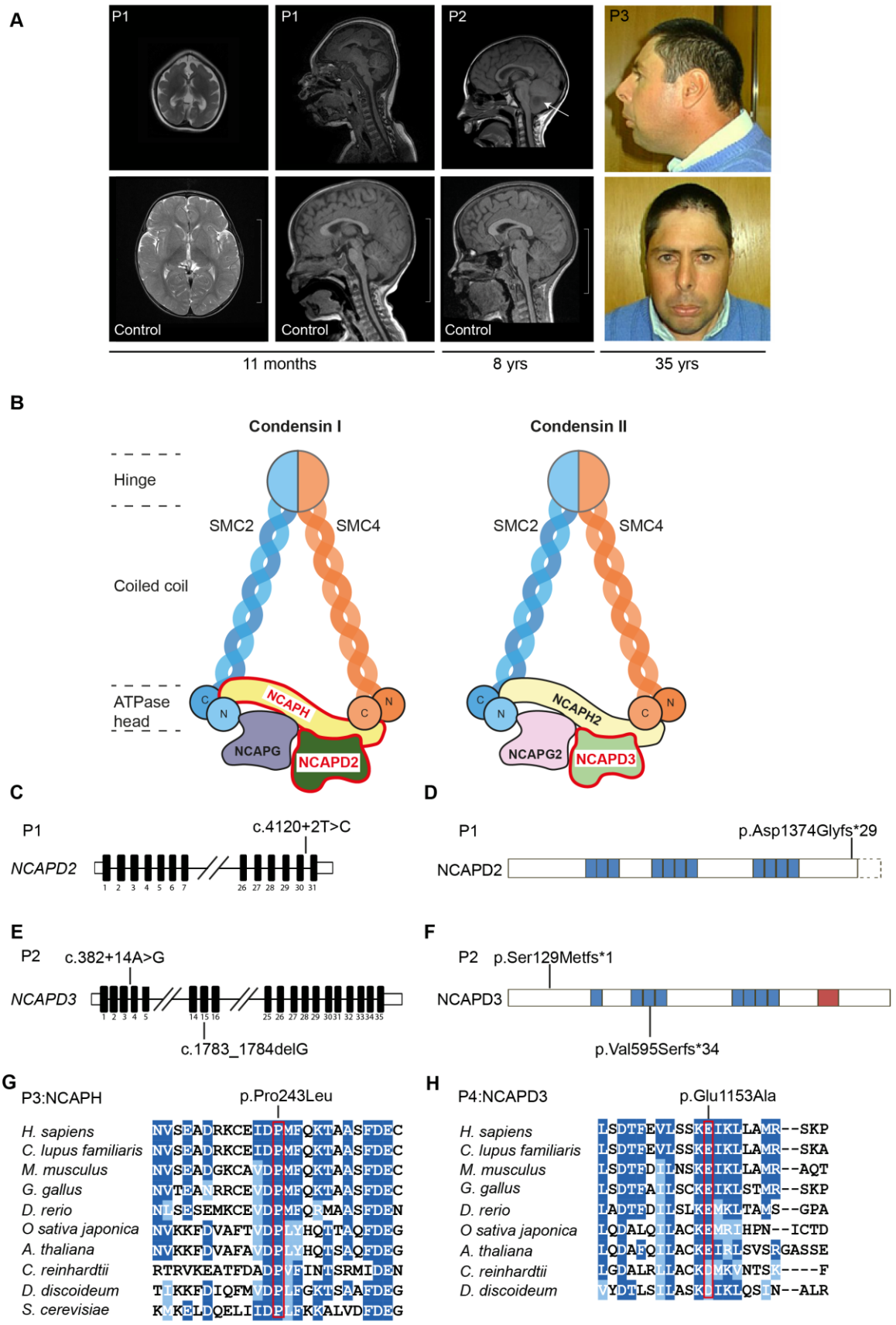
A
P1
P1
P2
P3
Control
Control
Control
11 months
8 yrs
35 yrs
B
Condensin I
Condensin II
Hinge
Coiled coil
ATPase head
SMC2
SMC4
SMC2
SMC4
NCAPH
NCAPG
NCAPD2
NCAPH2
NCAPG2
NCAPD3
C
P1
c.4120+2T>C
NCAPD2
D
P1
p.Asp1374Glyfs*29
NCAPD2
E
P2
c.382+14A>G
NCAPD3
c.1783_1784delG
F
P2
p.Ser129Metfs*1
NCAPD3
p.Val595Serfs*34
G
P3:NCAPH
p.Pro243Leu
H. sapiens
C. lupus familiaris
M. musculus
G. gallus
D. rerio
O sativa japonica
A. thaliana
C. reinhardtii
D. discoideum
S. cerevisiae
H
P4:NCAPD3
p.Glu1153Ala
H. sapiens
C. lupus familiaris
M. musculus
G. gallus
D. rerio
O sativa japonica
A. thaliana
C. reinhardtii
D. discoideum

Figure 1. Mutations in condensin I and II subunits cause microcephaly

(A) Reduced cerebral cortex size is seen in individuals with mutations in condensin subunits. Left, axial (T2-weighted) and sagittal (T1) MRI images from P1 at 11 months age and P2, Sagittal (T1) aged 8 years, 8 months, compared with age-matched controls. Arrow, low signal area within cerebellum corresponding to site of medulloblastoma. Scale bar 10cm. Left, photographs demonstrating reduced occipitofrontal circumference and sloping forehead in patient P3.

(B) Schematic of condensin I and II complexes with subunits containing patient mutations highlighted by red-edge boxes. Both condensins contain five subunits, sharing the same two core SMC subunits (2 & 4) which dimerize at the hinge domain. Each SMC subunit is composed of two coiled coil domains extending from the hinge domain forming an antiparallel coil which ends in an ATPase head domain. The two complexes then differ in the three non-SMC subunits: A kleisin protein (NCAPH in condensin I, NCAPH2 in condensin II) bridges the ATPase head domains of the two SMC subunits and two HEAT repeat proteins (NCAPG & NCAPD2 in condensin I, NCAPG2 & NCAPD3 in condensin II) associate with the complex predominantly through interactions with the kleisin subunit.

(C-F) Schematics of *NCAPD2* and *NCAPD3* genes and encoded proteins, depicting mutations identified in P1 and P2. **(C)** A homozygous essential splice site mutation is present in *NCAPD2* in P1, **(D)** predicted to alter the C-terminus of the protein. **(E)** Compound heterozygous mutations in P2, and **(F)** their predicted protein consequences. Coding exons, black; UTRs white boxes. HEAT repeats in blue boxes, coiled coil regions in red (Ono et al. 2003).

(G,H) Missense mutations in P3, P4 disrupt highly conserved amino acid residues. **(G)** The codon disrupted by the *NCAPH* Pro243Leu substitution is conserved in eukaryotes. **(H)** Amino acid 1153 is strongly conserved in condensin II NCAPD3 subunits across animal kingdoms. Alignment of species with complete condensin II complexes demonstrates that many metozoa and plants retain a glutamate at the mutated site in NCAPD3 in P4, while in Amoebazoa (Dictyostelium discoideum) and green algae (Chlamydomonas reinhardtii) a physiochemically similar aspartate residue is present. Not all model organisms are shown, as some eukaryotes such as fungi and yeast only possess a single condensin complex (Hirano 2012), and use of condensin complexes in invertebrates varies (Savvidou et al. 2005). Residues dark blue >60% identical, light blue similar.

Martin_Fig2

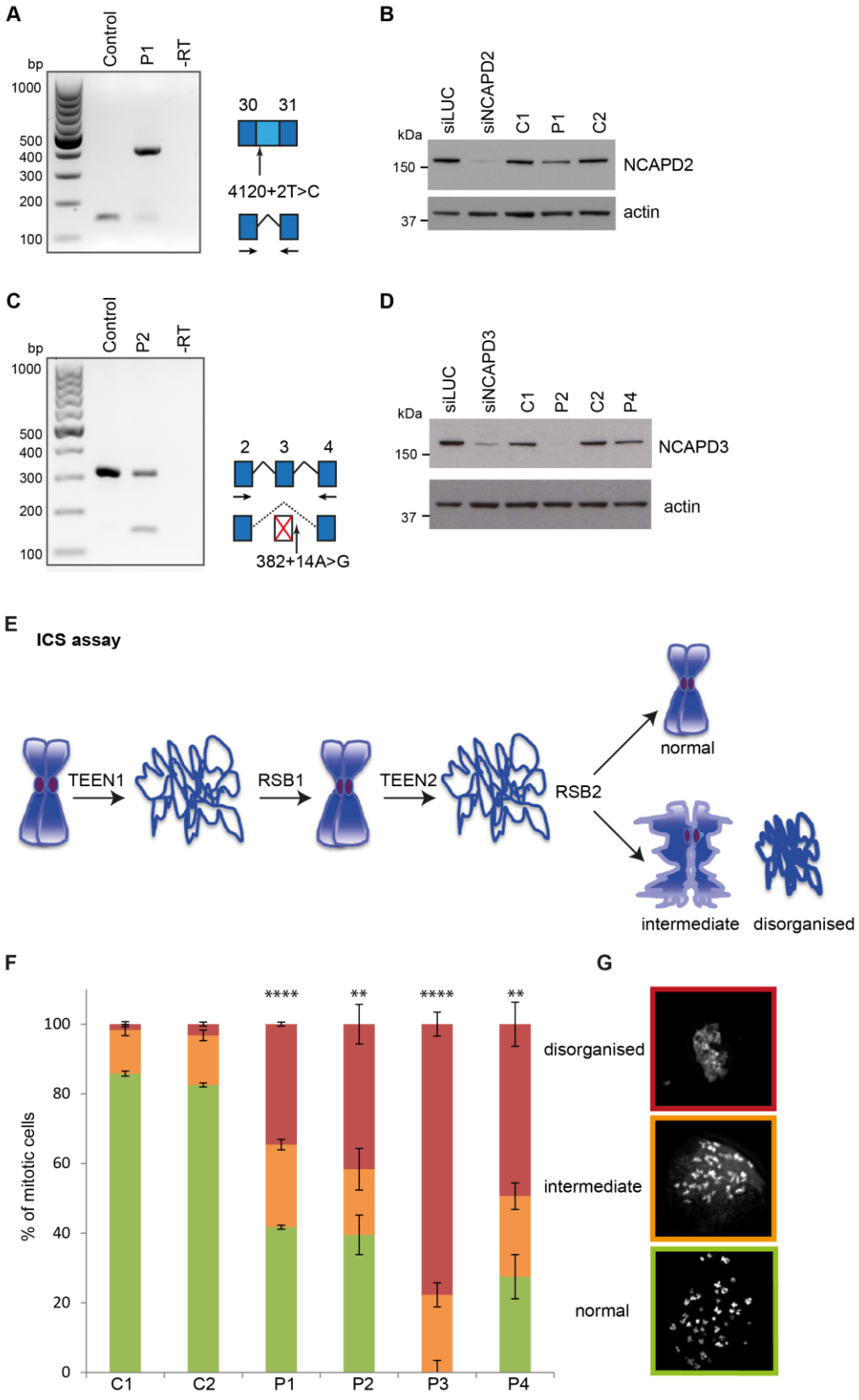
A
Control
P1
-RT
bp
1000
500
400
300
200
100
30
31
4120+2T>C
B
siLUC
siNCAPD2
C1
P1
C2
kDa
150
NCAPD2
37
actin
C
Control
P2
-RT
bp
1000
500
400
300
200
100
2
3
4
382+14A>G
D
siLUC
siNCAPD3
C1
P2
C2
P4
kDa
150
NCAPD3
37
actin
E
ICS assay
TEEN1
RSB1
TEEN2
RSB2
normal
intermediate
disorganised
F
% of mitotic cells
100
80
60
40
20
0
****
**
****
**
C1
C2
P1
P2
P3
P4
G
disorganised
intermediate
normal

Figure 2. Mutations impair canonical condensin function in mitotic chromosome compaction

(A,B) The c.4120 + 2T>C mutation results in retention of intron 30 in *NCAPD2* transcripts and reduced NCAPD2 protein levels. **(A)** RT-PCR using primers in exon 30 and 31 (arrows, schematic) demonstrated altered splicing of *NCAPD2* in P1 fibroblasts. The larger 413 bp PCR product corresponded to a transcript containing intron 30, confirmed by subcloning and Sanger sequencing. This transcript encodes an alternative C-terminus comprising an additional 29 amino acids before a premature termination codon with consequent loss of 28 amino acids encoded by exon 31. **(B)** NCAPD2 protein levels are reduced in P1 fibroblasts. Immunoblot with anti-NCAPD2 antibody. Left two lanes, RNAi of *NCAPD2* in RPE1 cells confirms specificity of NCAPD2 antibody. Remaining lanes; P1 and control primary fibroblasts. NCAPD2 protein mobility is not expected to be altered in patient P1 as the mutant protein has a similar molecular weight to wild-type. Lower panel; loading control, blot probed with anti-actin antibody.

(C,D) The *NCAPD3* c.382 + 14A>G mutation leads to skipping of exon 3, that in combination with c.1783_1784delG frameshift mutation in trans, results in markedly reduced NCAPD3 protein. **(C)** Alternative splicing of *NCAPD3* in P2 fibroblasts, detected by RT-PCR using primers in exon 2 and exon 4 (arrows, schematic). The wild-type transcript represented by a PCR product of 317 bp is substantially reduced in P2 patient cells, while the smaller PCR fragment of 154 bp is only detectable in P2, and corresponds to a transcript in which exon 3 had been skipped (confirmed by subcloning and sequencing). This results in an out of frame transcript, expected to be subject to NMD. **(D)** Immunoblotting of NCAPD3 establishes that protein levels are markedly reduced in P2. Left two lanes; RNAi of *NCAPD3* in RPE1 cells demonstrating specificity of NCAPD3 antibody. Remaining lanes; patient and control primary fibroblasts. NCAPD3 protein is substantially depleted in P2, whereas protein levels are unaffected by the p.Glu1153Ala missense mutation in P4 fibroblasts. Lower panel; loading control, blot probed with anti-actin antibody.

(E) Schematic of intrinsic chromosome structure (ICS) assay. Sequential TEEN decompaction and refolding in RSB buffer is utilised to establish the structural integrity of mitotic chromosomes. **(F,G)** Patient mutations lead to compromised intrinsic chromosome structure. **(F)** Quantification of abnormal chromosome refolding after ICS assay in C1, C2 and P1-P4 patient cell fibroblasts (expt=3; n>30 mitoses/sample/experiment). Error bars, s.e.m. P-value, two-tailed t-test, ** ≤0.01, ****≤0.0001, proportion of 'disorganised' chromosomes versus C2. **(G)** Representative images of chromosome morphology from ICS assay. Chromosomes were visualised with DAPI following two sequential rounds of decompaction (TEEN) and refolding (RSB). Patient and control primary fibroblast chromosomes were scored as either reforming the original chromosome morphology ('normal'), partially reforming starting chromosome morphology ('intermediate') or complete loss of chromosome compaction ('disorganised').

Martin_Fig3

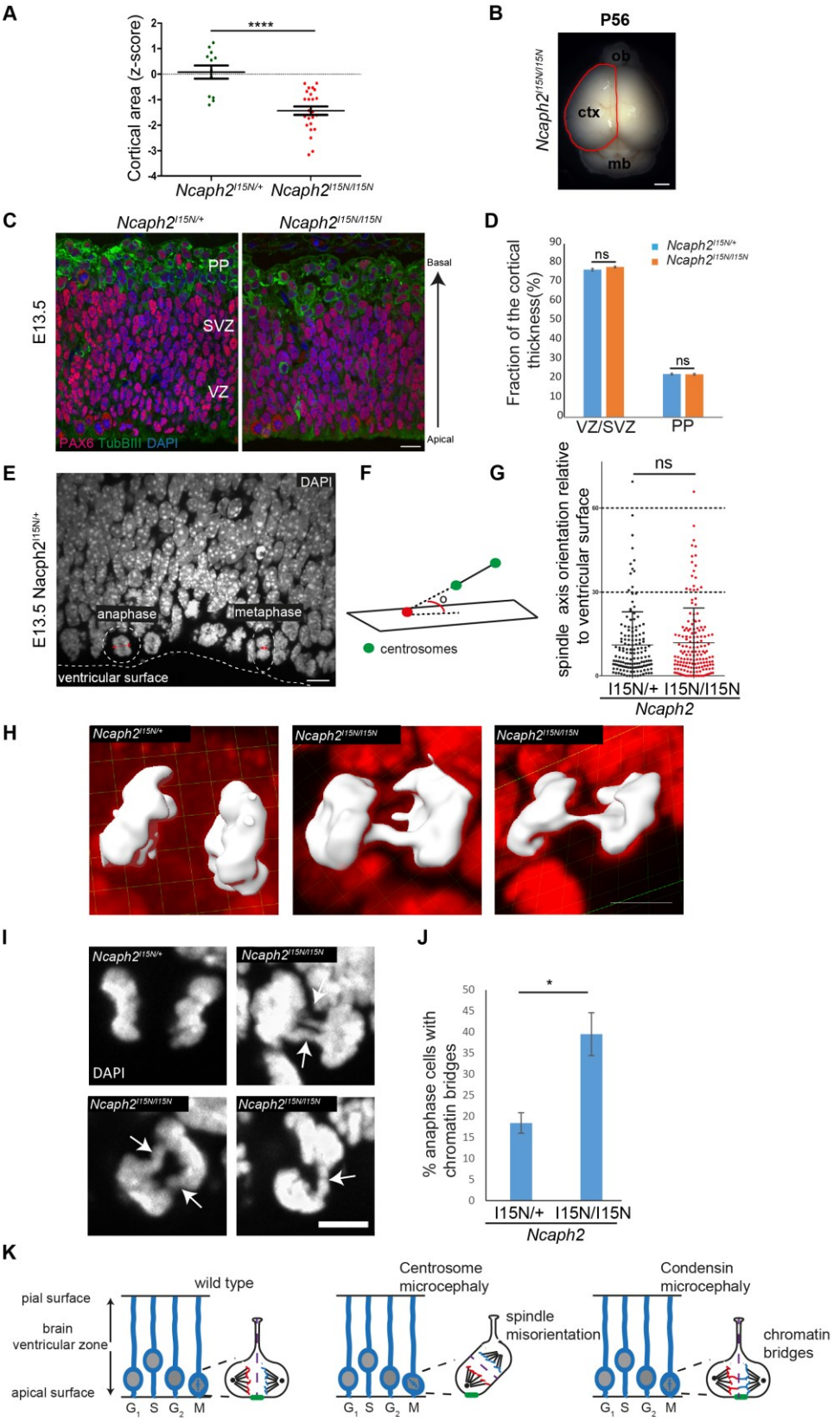
A
Cortical area (z-score)
****
Ncaph2I15N/+ Ncaph2I15N/I15N
B
P56
ob
ctx
mb
Ncaph2I15N/I15N
C
Ncaph2I15N/+
Ncaph2I15N/I15N
E13.5
PP
SVZ
VZ
PAX6 TubBIII DAPI
Basal
Apical
D
Fraction of the cortical thickness(%)
ns
Ncaph2I15N/+
Ncaph2I15N/I15N
VZ/SVZ
PP
E
E13.5 Nacph2I15N/+
DAPI
anaphase
metaphase
ventricular surface
F
centrosomes
G
spindle axis orientation relative to ventricular surface
ns
I15N/+ I15N/I15N
Ncaph2
H
Ncaph2I15N/+
Ncaph2I15N/I15N
Ncaph2I15N/I15N
I
Ncaph2I15N/+
DAPI
Ncaph2I15N/I15N
Ncaph2I15N/I15N
Ncaph2I15N/I15N
J
% anaphase cells with chromatin bridges
*
I15N/+ I15N/I15N
Ncaph2
K
wild type
pial surface
brain ventricular zone
apical surface
G1 S G2 M
Centrosome microcephaly
spindle misorientation
Condensin microcephaly
chromatin bridges

Figure 3. Impaired chromosome segregation instead of altered neural progenitor cleavage plane accounts for reduced cortical size in *Ncaph2*$^{l15N/l15N}$ mice

(A,B) Cerebral cortex surface area is reduced in *Ncaph2*$^{l15N/l15N}$ mice at 8 weeks. **(A)** Quantification of cortical area expressed as a z-score at 8 weeks age. n>12 mice per genotype, error bars, s.e.m. P value, two-tailed t-test, ****≤0.0001, versus littermate *Ncaph2*$^{l15N/+}$ mice. **(B)** Cortical area measurement. Red line indicates region measured of the dorsal cerebral cortex. Scale bar = 1.5mm. z-score defined as the standard deviations from the mean of age and sex-matched *Ncaph2*$^{l15N/+}$ mice at 8 weeks.

(C,D) The relative proportion of progenitor cells and neurons is retained during neurogenesis in *Ncaph2*$^{l15N/l15N}$ mice. **(C)** Representative images of neurogenesis in E13.5 *Ncaph2*$^{l15N/+}$ and *Ncaph2*$^{l15N/l15N}$ coronal sections immunostained for PAX6 (radial glia, red), TUBβIII (neurons, green) and DAPI (DNA, blue). **(D)** Quantification of proportions of TUBβIII and PAX6 positive cells per radial unit, determined by measurement of the thickness of the preplate (PP); and subventricular/ventricular zones (SVZ/VZ) respectively. Measurements made at 4 regions per coronal section for 2 coronal sections at equivalent rostro-caudal positions per brain, n=10 brains analysed for *Ncaph2*$^{l15N/+}$ and n=9 brains analysed for *Ncaph2*$^{l15N/l15N}$. Error bars, sem. Graph ns= non-significant with an unpaired t- test. Scale bar= 10μm

(E-G) Cleavage plane orientation is not affected in E13.5 *Ncaph2*$^{l15N/l15N}$ mice. **(E)** Representative image of mitotic apical progenitors, illustrating normal orientation of mitotic spindle parallel to ventricular surface. E13.5 coronal sections, nuclei (DAPI,white). Dashed line, ventricular surface; dashed circles, mitotic cells and double side arrows represent the axis of the mitotic spindle and position of mitotic centrosomes (identified by Aurora A immunostaining). Scale bar=10μm. **(F)** Schematic outlining measurement of mitotic spinde axis, defined as the angle between the spindle line vector and the reference plane for the ventricular surface. Green circles, centrosomes; red circle, point where spindle line vector intersects the plane of the ventricular surface. **(G)** Quantification of mitotic spindle orientation in apical neural progenitors at metaphase and anaphase in E13.5 neuroepithelium. *Ncaph*$^{2l15N/+}$ mice (black circles, mean angle 11°, n=150 cells from 3 brains) and Ncaph2$^{l15N/l15N}$ mice (red circles, mean angle 12°, n=159 cells from 3 brains). Error bars, sd. p=0.56 with an unpaired t- test.

(H-J) Chromosome segregation is impaired in E13.5 *Ncaph2*$^{l15N/l15N}$ apical neural progenitors. **(H, I)** Representative images of chromatin bridges in anaphase apical progenitor cells. **(H)** 3D reconstructions (DAPI stain, red, anaphase cell DNA highlighted in white, scale bar = 4 μm) and **(I)** 2D DAPI stained confocal sections (scale bar=5 μm) from E13.5 coronal sections. **(J)** Quantification of chromatin bridges observed in apical progenitors of E13.5 *Ncaph2*$^{l15N/+}$ and *Ncaph2*$^{l15N/l15N}$ mice. Significantly increased numbers of mid and late anaphase cells with chromatin bridges are observed in *Ncaph2*$^{l15N/l15N}$ mice (n=46 cells from 3 brains) compared to *Ncaph*$^{2l15N/+}$ mice (n=72 cells from 3 brains). Error bars, s.e.m. P value, two-tailed t-test, =0.02 versus *Ncaph*$^{2l15N/+}$ mice.

(K) Model: During early neurogenesis, neural stem cells divide symmetrically to enlarge the pool of neural progenitors. Mitosis occurs at the ventricular surface with the axis of the mitotic spindle parallel to this surface. This ensures that the cleavage furrow is perpendicular and that consequently basal fate determinants (indicated by green bar) segregate equally between daughter cells ensuring retention of stem cell identity. Middle panel, the mitotic spindle fails to align when genes encoding centrosomal proteins are mutated (ASPM, CDK5RAP2, MCPH1, CPAP) leading to oblique cell cleavage events that result in premature asymmetric cell division. Daughter neuron cells are produced and expansion of the neural stem cell pool is decreased, consequently reducing the total number of neurons. Right panel, in contrast, condensin mutations lead to chromatin bridges during neurogenesis with unaltered spindle orientation. Such chromosome segregation errors would be expected to reduce cell proliferation and survival, depleting neuronal number generated during neurogenesis.

Martin_Fig4

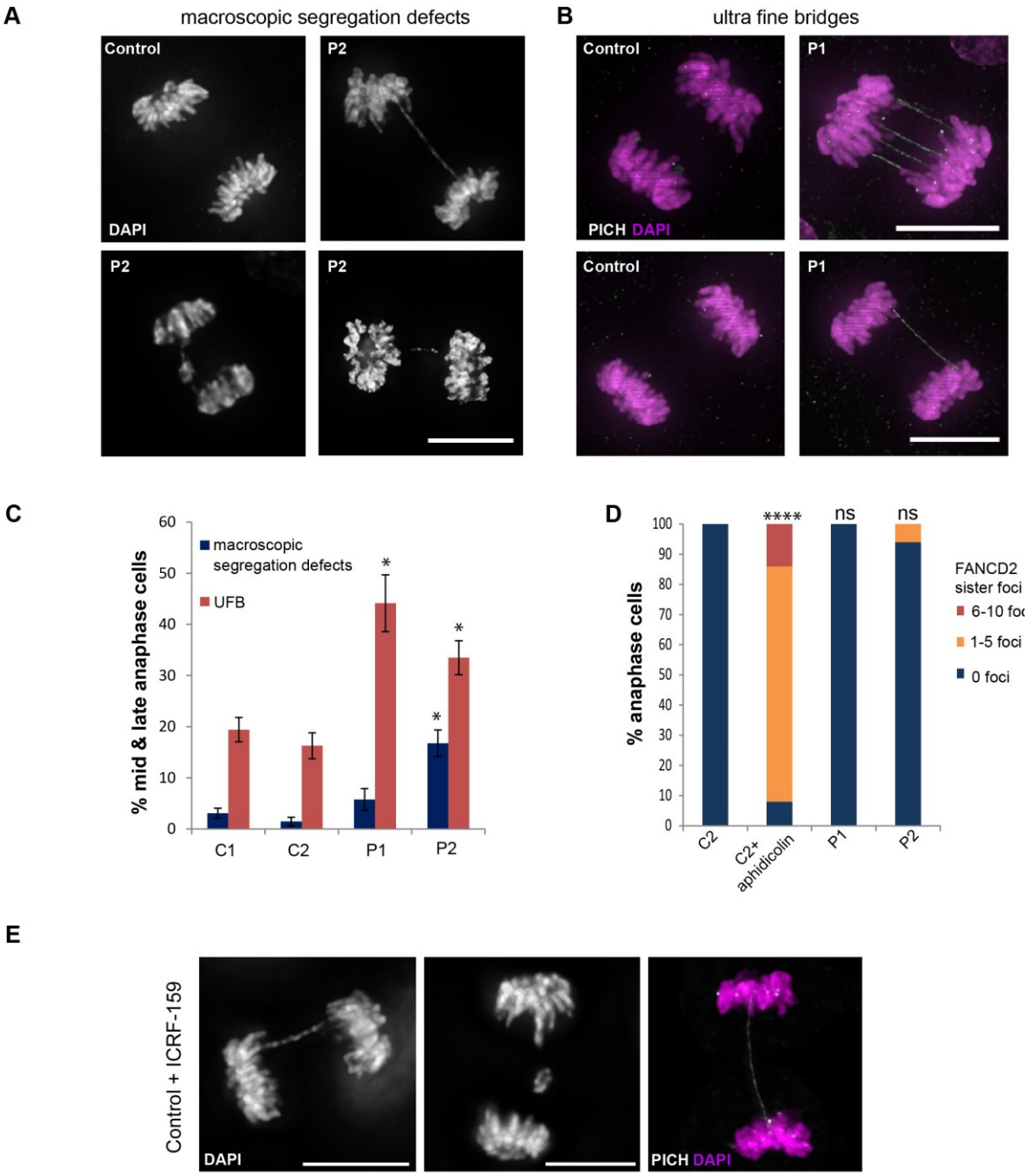
A
macroscopic segregation defects
Control
P2
DAPI
P2
P2
B
ultra fine bridges
Control
P1
PICH DAPI
Control
P1
C
% mid & late anaphase cells
macroscopic segregation defects
UFB
C1
C2
P1
P2
D
% anaphase cells
****
ns
ns
FANCD2 sister foci
6-10 foc
1-5 foci
0 foci
C2
C2+ aphidicolin
P1
P2
E
Control + ICRF-159
DAPI
PICH DAPI

Figure 4. Condensin patient mutations lead to decatenation failure at mitosis

(A-C) Chromosome segregation is impaired in patient P1 (NCAPD2) and P2 (NCAPD3) primary fibroblasts. Representative images of **(A)** chromatin bridges and lagging chromosomes/chromosome fragments detected with DAPI stain (macroscopic chromosome segregation defects), and **(B)** UFBs were detected by presence of PICH and absence of DAPI stain. Scale bars=10μm. **(C)** Quantification of macroscopic chromosome segregation defects, defined as DAPI positive chromatin bridges, lagging chromosomes or chromosome fragments; and UFBs, scored in anaphase C1, C2, patient P1 and P2 fibroblasts. Increased numbers of mid and late anaphase cells with UFBs are seen in NCAPD2 P1 and NCAPD3 P2 patient cell fibroblasts (expt≥3, n>50 anaphases/sample/expt) and P2 fibroblasts also had elevated macroscopic chromosome segregation defects compared to Control 1 and 2 fibroblasts (exp ≥3, n>100). Error bars, s.e.m. P value, two-tailed t-test, *≤0.05 versus C1.

(D) UFBs in condensin patient cells do not arise from late replication intermediates. Quantification of the number of FANCD2 sister foci during anaphase in C2, P1 and P2 fibroblasts. C2 fibroblasts treated with 0.1μM aphidicolin for 16 hrs to induce late replication intermediates through replication stress was also included as a positive control (n=50 cells, exp=1)

(E) Chromosome decatenation failure due to topoisomerase II α inhibition in control fibroblasts results in identical chromosome segregation defects as those observed in condensin patient cells. Representative images of bulky chromatin bridges and lagging chromatin detected with DAPI stain and UFBs detected by PICH stain. Scale bars=10 μm. C2 fibroblasts were treated with 5 μM ICRF-159 for 24 hr.

Martin_Fig5

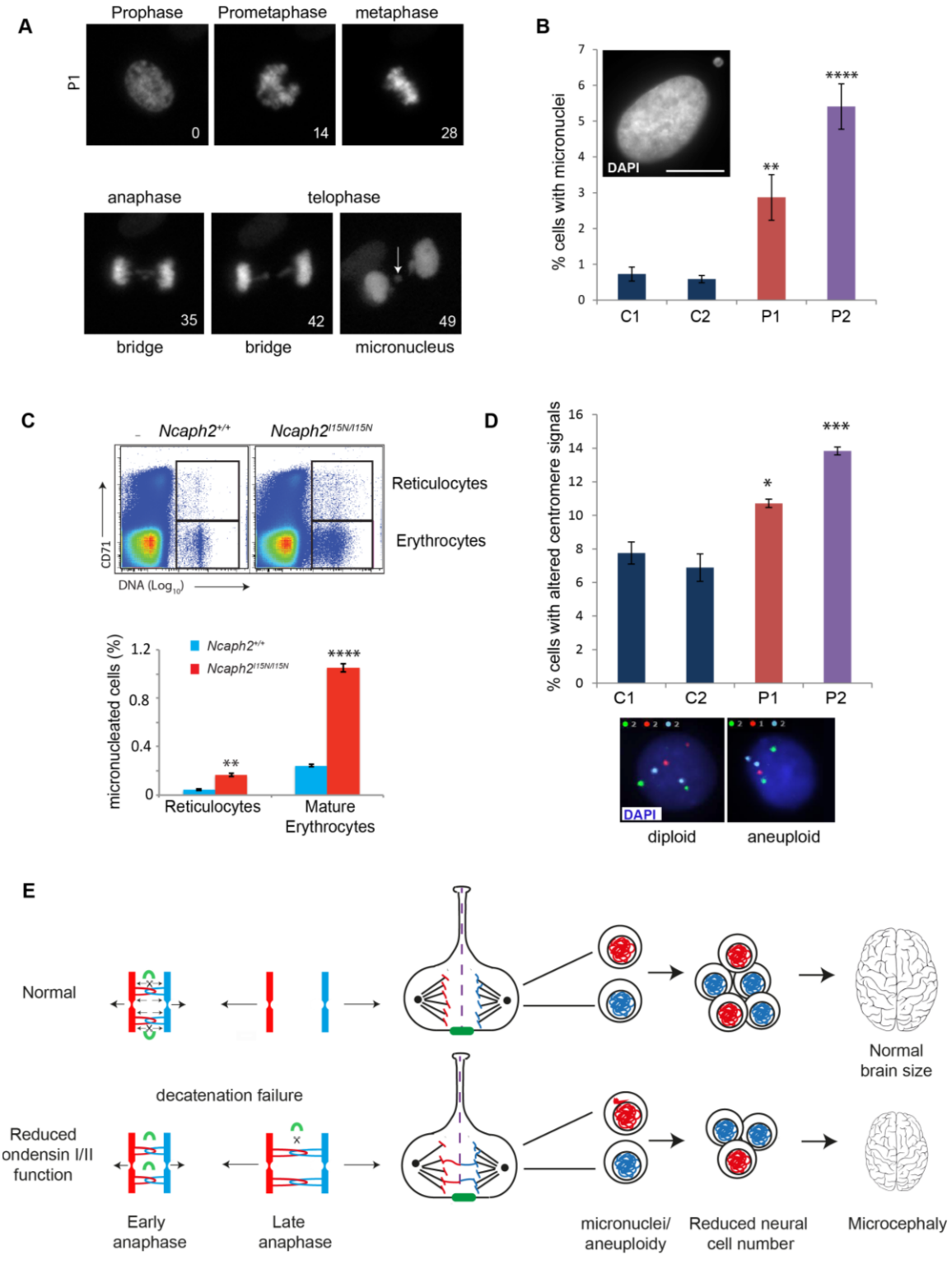
A
Prophase
Prometaphase
metaphase
P1
0
14
28
anaphase
telophase
35
42
49
bridge
bridge
micronucleus
B
% cells with micronuclei
DAPI
**
****
C1
C2
P1
P2
C
Ncaph2+/+
Ncaph2I15N/I15N
Reticulocytes
Erythrocytes
CD71
DNA (Log10)
micronucleated cells (%)
Reticulocytes
Mature Erythrocytes
D
% cells with altered centromere signals
*
***
DAPI
diploid
aneuploid
E
Normal
decatenation failure
Reduced condensin I/II function
Early anaphase
Late anaphase
micronuclei/ aneuploidy
Reduced neural cell number
Normal brain size
Microcephaly

Figure 5. Decatenation failure results in micronuclei and aneuploidy in condensin mouse and patient cells

(A) Live imaging stills of chromatin bridge and subsequent micronuclei formation in a P1 patient fibroblast cell. DNA visualised by transient expression of RFP tagged histone 2B. Time is shown in minutes from nuclear envelope breakdown. Arrow indicates position of micronucleus.

(B) NCAPD2 P1 and NCAPD3 P2 fibroblasts have significantly elevated levels of micronuclei. Percentage of micronuclei positive cells quantified (expt=5, n>500 cells). Error bars, s.e.m. P value, two-tailed t-test, ** ≤0.01, ****≤0.0001, versus C1. Inset, representative picture of P2 patient fibroblast cell with micronucleus (top right corner). Scale bar=10μm.

(C) Elevated frequency of micronuclei in peripheral blood of *Ncaph2*$^{I15N/I15N}$ mice. Top panel, representative FACS plots of CD71 (reticuloctyte marker) versus propidium iodide (DNA content) of *Ncaph2*$^{I15N/I15N}$ and *Ncaph2*$^{+/+}$ adult mice demonstrating gating strategy. Gated cells have sub-diploid DNA content (micronuclei). Upper gate, micronuclei in CD71+ve reticulocytes and lower gate, micronuclei in mature erythrocytes. In contrast to the usual linear scale for DNA content FACS plots, the DNA axis is presented on a Log_{10} scale, with fully nucleated cells off the scale, and micronucleated cells appearing to the right of enucleated cells, within the gates indicated by the boxed regions. Right panel, quantification of flow cytometry analysis of micronuclei in the peripheral blood reticulocytes and mature erythrocytes of *Ncaph2*$^{I15N/I15N}$ and *Ncaph2*$^{+/+}$ adult mice. N= 3, error bars, s.e.m. P value, two-tailed t-test, **≤0.01, ****≤0.0001, versus *Ncaph2*$^{+/+}$ mice.

(D) Levels of aneuploidy are significantly increased in NCAPD2 P1 and NCAPD3 P2 fibroblasts. Upper panel, quantification of the percentage of cells with numerical chromosome imbalances detected by interphase FISH (bars= average of two sets of probes detecting chromosome 3, 7 and 18 and 4, 10 and 17 respectively; exp≥4, n>700 cells). Error bars, s.e.m. P value, two-tailed t-test, * ≤0.05, ***≤0.001, versus C1. Lower panel, representative images of interphase FISH of chromosomes 4 (green), 10 (red) and 17 (aqua) in primary fibroblasts.

(E) Model: Decatenation failure in condensin-deficient neural stem cells reduces brain size through a reduction in cell number generated during neurogenesis. Impaired mitotic chromosome compaction in condensin deficient neural stem cells decreases tension in catenated DNA reducing topIIα DNA strand exchange activity (TopIIα enzyme indicated by green curved line). This delays decatenation of DNA between sister chromatids leading to increased chromosome segregation errors and subsequent aneuploidy/micronuclei formation. Anueploidy in condensin-deficient neural stem cells (NSC) is likely to reduce cell number by impaired proliferation potential (Gogendeau et al. 2015) and/or reduced cell survival (Marthiens et al. 2013; Nishide and Hirano 2014) during the restricted developmental window of neurogenesis.

References

Al-Dosari, M.S., Shaheen, R., Colak, D., and Alkuraya, F.S. 2010. Novel CENPJ mutation causes Seckel syndrome. *J Med Genet* **47**(6): 411-414.

Baumann, C., Korner, R., Hofmann, K., and Nigg, E.A. 2007. PICH, a centromere-associated SNF2 family ATPase, is regulated by Plk1 and required for the spindle checkpoint. *Cell* **128**(1): 101-114.

Baxter, J., Sen, N., Martinez, V.L., De Carandini, M.E., Schvartzman, J.B., Diffley, J.F., and Aragon, L. 2011. Positive supercoiling of mitotic DNA drives decatenation by topoisomerase II in eukaryotes. *Science* **331**(6022): 1328-1332.

Bicknell, L.S., Bongers, E.M., Leitch, A., Brown, S., Schoots, J., Harley, M.E., Aftimos, S., Al-Aama, J.Y., Bober, M., Brown, P.A., van Bokhoven, H., Dean, J., Edrees, A.Y., Feingold, M., Fryer, A., Hoefsloot, L.H., Kau, N., Knoers, N.V., Mackenzie, J., Opitz, J.M., Sarda, P., Ross, A., Temple, I.K., Toutain, A., Wise, C.A., Wright, M., and Jackson, A.P. 2011. Mutations in the pre-replication complex cause Meier-Gorlin syndrome. *Nat Genet* **43**(4): 356-359.

Bond, J., Roberts, E., Mochida, G.H., Hampshire, D.J., Scott, S., Askham, J.M., Springell, K., Mahadevan, M., Crow, Y.J., Markham, A.F., Walsh, C.A., and Woods, C.G. 2002. ASPM is a major determinant of cerebral cortical size. *Nat Genet* **32**(2): 316-320.

Bond, J., Roberts, E., Springell, K., Lizarraga, S.B., Scott, S., Higgins, J., Hampshire, D.J., Morrison, E.E., Leal, G.F., Silva, E.O., Costa, S.M., Baralle, D., Raponi, M., Karbani, G., Rashid, Y., Jafri, H., Bennett, C., Corry, P., Walsh, C.A., and Woods, C.G. 2005. A centrosomal mechanism involving CDK5RAP2 and CENPJ controls brain size. *Nat Genet* **37**(4): 353-355.

Chan, K.L., North, P.S., and Hickson, I.D. 2007. BLM is required for faithful chromosome segregation and its localization defines a class of ultrafine anaphase bridges. *Embo J* **26**(14): 3397-3409.

Chan, K.L., Palmai-Pallag, T., Ying, S., and Hickson, I.D. 2009. Replication stress induces sister-chromatid bridging at fragile site loci in mitosis. *Nat Cell Biol* **11**(6): 753-760.

Charbin, A., Bouchoux, C., and Uhlmann, F. 2014. Condensin aids sister chromatid decatenation by topoisomerase II. *Nucleic Acids Res* **42**(1): 340-348.

Crasta, K., Ganem, N.J., Dagher, R., Lantermann, A.B., Ivanova, E.V., Pan, Y., Nezi, L., Protopopov, A., Chowdhury, D., and Pellman, D. 2012. DNA breaks and chromosome pulverization from errors in mitosis. *Nature* **482**(7383): 53-58.

Crow, Y.J., Leitch, A., Hayward, B.E., Garner, A., Parmar, R., Griffith, E., Ali, M., Semple, C., Aicardi, J., Babul-Hirji, R., Baumann, C., Baxter, P., Bertini, E., Chandler, K.E., Chitayat, D., Cau, D., Dery, C., Fazzi, E., Goizet, C., King, M.D., Klepper, J., Lacombe, D., Lanzi, G., Lyall, H., Martinez-Frias, M.L., Mathieu, M., McKeown, C., Monier, A., Oade, Y., Quarrell, O.W., Rittey, C.D., Rogers, R.C., Sanchis, A., Stephenson, J.B., Tacke, U., Till, M., Tolmie, J.L., Tomlin, P., Voit, T., Weschke, B., Woods, C.G., Lebon, P., Bonthron, D.T., Ponting, C.P., and Jackson, A.P. 2006. Mutations in genes encoding ribonuclease H2 subunits cause Aicardi-Goutieres syndrome and mimic congenital viral brain infection. *Nature genetics* **38**(8): 910-916.

Cuylen, S. and Haering, C.H. 2011. Deciphering condensin action during chromosome segregation. *Trends Cell Biol* **21**(9): 552-559.

D'Ambrosio, C., Kelly, G., Shirahige, K., and Uhlmann, F. 2008. Condensin-dependent rDNA decatenation introduces a temporal pattern to chromosome segregation. *Curr Biol* **18**(14): 1084-1089.

Deardorff, M.A., Kaur, M., Yaeger, D., Rampuria, A., Korolev, S., Pie, J., Gil-Rodriguez, C., Arnedo, M., Loeys, B., Kline, A.D., Wilson, M., Lillquist, K., Siu, V., Ramos, F.J., Musio, A., Jackson, L.S., Dorsett, D., and Krantz, I.D. 2007. Mutations in cohesin complex members SMC3 and SMC1A cause a mild variant of cornelia de Lange syndrome with predominant mental retardation. *Am J Hum Genet* **80**(3): 485-494.

Deardorff, M.A., Wilde, J.J., Albrecht, M., Dickinson, E., Tennstedt, S., Braunholz, D., Monnich, M., Yan, Y., Xu, W., Gil-Rodriguez, M.C., Clark, D., Hakonarson, H., Halbach, S., Michelis, L.D.,

Rampuria, A., Rossier, E., Spranger, S., Van Maldergem, L., Lynch, S.A., Gillessen-Kaesbach, G., Ludecke, H.J., Ramsay, R.G., McKay, M.J., Krantz, I.D., Xu, H., Horsfield, J.A., and Kaiser, F.J. 2012. RAD21 mutations cause a human cohesinopathy. *Am J Hum Genet* **90**(6): 1014-1027.

Deciphering Developmental Disorders, S. 2015. Large-scale discovery of novel genetic causes of developmental disorders. *Nature* **519**(7542): 223-228.

Dorsett, D. 2011. Cohesin: genomic insights into controlling gene transcription and development. *Curr Opin Genet Dev* **21**(2): 199-206.

Fish, J.L., Kosodo, Y., Enard, W., Paabo, S., and Huttner, W.B. 2006. Aspm specifically maintains symmetric proliferative divisions of neuroepithelial cells. *Proc Natl Acad Sci U S A* **103**(27): 10438-10443.

Freeman, J.V., Cole, T.J., Chinn, S., Jones, P.R., White, E.M., and Preece, M.A. 1995. Cross sectional stature and weight reference curves for the UK, 1990. *Arch Dis Child* **73**(1): 17-24.

Gerlich, D., Hirota, T., Koch, B., Peters, J.M., and Ellenberg, J. 2006. Condensin I stabilizes chromosomes mechanically through a dynamic interaction in live cells. *Curr Biol* **16**(4): 333-344.

Gogendeau, D., Siudeja, K., Gambarotto, D., Pennetier, C., Bardin, A.J., and Basto, R. 2015. Aneuploidy causes premature differentiation of neural and intestinal stem cells. *Nat Commun* **6**: 8894.

Gosling, K.M., Makaroff, L.E., Theodoratos, A., Kim, Y.H., Whittle, B., Rui, L., Wu, H., Hong, N.A., Kennedy, G.C., Fritz, J.A., Yates, A.L., Goodnow, C.C., and Fahrer, A.M. 2007. A mutation in a chromosome condensin II subunit, kleisin beta, specifically disrupts T cell development. *Proc Natl Acad Sci U S A* **104**(30): 12445-12450.

Green, L.C., Kalitsis, P., Chang, T.M., Cipetic, M., Kim, J.H., Marshall, O., Turnbull, L., Whitchurch, C.B., Vagnarelli, P., Samejima, K., Earnshaw, W.C., Choo, K.H., and Hudson, D.F. 2012. Contrasting roles of condensin I and condensin II in mitotic chromosome formation. *J Cell Sci* **125**(Pt 6): 1591-1604.

Griffith, E., Walker, S., Martin, C.A., Vagnarelli, P., Stiff, T., Vernay, B., Al Sanna, N., Saggar, A., Hamel, B., Earnshaw, W.C., Jeggo, P.A., Jackson, A.P., and O'Driscoll, M. 2008. Mutations in pericentrin cause Seckel syndrome with defective ATR-dependent DNA damage signaling. *Nat Genet* **40**(2): 232-236.

Gruber, R., Zhou, Z., Sukchev, M., Joerss, T., Frappart, P.O., and Wang, Z.Q. 2011. MCPH1 regulates the neuroprogenitor division mode by coupling the centrosomal cycle with mitotic entry through the Chk1-Cdc25 pathway. *Nat Cell Biol* **13**(11): 1325-1334.

Hagstrom, K.A., Holmes, V.F., Cozzarelli, N.R., and Meyer, B.J. 2002. C. elegans condensin promotes mitotic chromosome architecture, centromere organization, and sister chromatid segregation during mitosis and meiosis. *Genes Dev* **16**(6): 729-742.

Hanks, S., Coleman, K., Reid, S., Plaja, A., Firth, H., Fitzpatrick, D., Kidd, A., Mehes, K., Nash, R., Robin, N., Shannon, N., Tolmie, J., Swansbury, J., Irrthum, A., Douglas, J., and Rahman, N. 2004. Constitutional aneuploidy and cancer predisposition caused by biallelic mutations in BUB1B. *Nat Genet* **36**(11): 1159-1161.

Haydar, T.F., Ang, E., Jr., and Rakic, P. 2003. Mitotic spindle rotation and mode of cell division in the developing telencephalon. *Proc Natl Acad Sci U S A* **100**(5): 2890-2895.

Hirano, T. 2012. Condensins: universal organizers of chromosomes with diverse functions. *Genes & development* **26**(15): 1659-1678.

Hirano, T., Kobayashi, R., and Hirano, M. 1997. Condensins, chromosome condensation protein complexes containing XCAP-C, XCAP-E and a Xenopus homolog of the Drosophila Barren protein. *Cell* **89**(4): 511-521.

Hirano, T. and Mitchison, T.J. 1994. A heterodimeric coiled-coil protein required for mitotic chromosome condensation in vitro. *Cell* **79**(3): 449-458.

Hirota, T., Gerlich, D., Koch, B., Ellenberg, J., and Peters, J.M. 2004. Distinct functions of condensin I and II in mitotic chromosome assembly. *J Cell Sci* **117**(Pt 26): 6435-6445.

Hoffelder, D.R., Luo, L., Burke, N.A., Watkins, S.C., Gollin, S.M., and Saunders, W.S. 2004. Resolution of anaphase bridges in cancer cells. *Chromosoma* **112**(8): 389-397.

Houlard, M., Godwin, J., Metson, J., Lee, J., Hirano, T., and Nasmyth, K. 2015. Condensin confers the longitudinal rigidity of chromosomes. *Nat Cell Biol* **17**(6): 771-781.

Hudson, D.F., Vagnarelli, P., Gassmann, R., and Earnshaw, W.C. 2003. Condensin is required for nonhistone protein assembly and structural integrity of vertebrate mitotic chromosomes. *Dev Cell* **5**(2): 323-336.

Insolera, R., Bazzi, H., Shao, W., Anderson, K.V., and Shi, S.H. 2014. Cortical neurogenesis in the absence of centrioles. *Nat Neurosci* **17**(11): 1528-1535.

Janssen, A., van der Burg, M., Szuhai, K., Kops, G.J., and Medema, R.H. 2011. Chromosome segregation errors as a cause of DNA damage and structural chromosome aberrations. *Science* **333**(6051): 1895-1898.

Juschke, C., Xie, Y., Postiglione, M.P., and Knoblich, J.A. 2014. Analysis and modeling of mitotic spindle orientations in three dimensions. *Proc Natl Acad Sci U S A* **111**(3): 1014-1019.

Kalay, E., Yigit, G., Aslan, Y., Brown, K.E., Pohl, E., Bicknell, L.S., Kayserili, H., Li, Y., Tuysuz, B., Nurnberg, G., Kiess, W., Koegl, M., Baessmann, I., Buruk, K., Toraman, B., Kayipmaz, S., Kul, S., Ikbal, M., Turner, D.J., Taylor, M.S., Aerts, J., Scott, C., Milstein, K., Dollfus, H., Wieczorek, D., Brunner, H.G., Hurles, M., Jackson, A.P., Rauch, A., Nurnberg, P., Karaguzel, A., and Wollnik, B. 2011. CEP152 is a genome maintenance protein disrupted in Seckel syndrome. *Nat Genet* **43**(1): 23-26.

Ke, Y., Huh, J.W., Warrington, R., Li, B., Wu, N., Leng, M., Zhang, J., Ball, H.L., and Yu, H. 2011. PICH and BLM limit histone association with anaphase centromeric DNA threads and promote their resolution. *Embo J* **30**(16): 3309-3321.

Klingseisen, A. and Jackson, A.P. 2011. Mechanisms and pathways of growth failure in primordial dwarfism. *Genes Dev* **25**(19): 2011-2024.

Lancaster, M.A., Renner, M., Martin, C.A., Wenzel, D., Bicknell, L.S., Hurles, M.E., Homfray, T., Penninger, J.M., Jackson, A.P., and Knoblich, J.A. 2013. Cerebral organoids model human brain development and microcephaly. *Nature* **501**(7467): 373-379.

Leiserson, M.D., Vandin, F., Wu, H.T., Dobson, J.R., Eldridge, J.V., Thomas, J.L., Papoutsaki, A., Kim, Y., Niu, B., McLellan, M., Lawrence, M.S., Gonzalez-Perez, A., Tamborero, D., Cheng, Y., Ryslik, G.A., Lopez-Bigas, N., Getz, G., Ding, L., and Raphael, B.J. 2015. Pan-cancer network analysis identifies combinations of rare somatic mutations across pathways and protein complexes. *Nat Genet* **47**(2): 106-114.

Lizarraga, S.B., Margossian, S.P., Harris, M.H., Campagna, D.R., Han, A.P., Blevins, S., Mudbhary, R., Barker, J.E., Walsh, C.A., and Fleming, M.D. 2010. Cdk5rap2 regulates centrosome function and chromosome segregation in neuronal progenitors. *Development* **137**(11): 1907-1917.

Lukas, C., Savic, V., Bekker-Jensen, S., Doil, C., Neumann, B., Pedersen, R.S., Grofte, M., Chan, K.L., Hickson, I.D., Bartek, J., and Lukas, J. 2011. 53BP1 nuclear bodies form around DNA lesions generated by mitotic transmission of chromosomes under replication stress. *Nat Cell Biol* **13**(3): 243-253.

Maciejowski, J., Li, Y., Bosco, N., Campbell, P.J., and de Lange, T. 2015. Chromothripsis and Kataegis Induced by Telomere Crisis. *Cell* **163**(7): 1641-1654.

Mannini, L., Cucco, F., Quarantotti, V., Krantz, I.D., and Musio, A. 2013. Mutation spectrum and genotype-phenotype correlation in Cornelia de Lange syndrome. *Human mutation* **34**(12): 1589-1596.

Marthiens, V., Rujano, M.A., Pennetier, C., Tessier, S., Paul-Gilloteaux, P., and Basto, R. 2013. Centrosome amplification causes microcephaly. *Nat Cell Biol* **15**(7): 731-740.

Martin, C.A., Ahmad, I., Klingseisen, A., Hussain, M.S., Bicknell, L.S., Leitch, A., Nurnberg, G., Toliat, M.R., Murray, J.E., Hunt, D., Khan, F., Ali, Z., Tinschert, S., Ding, J., Keith, C., Harley, M.E.,

Heyn, P., Muller, R., Hoffmann, I., Daire, V.C., Dollfus, H., Dupuis, L., Bashamboo, A., McElreavey, K., Kariminejad, A., Mendoza-Londono, R., Moore, A.T., Saggar, A., Schlechter, C., Weleber, R., Thiele, H., Altmuller, J., Hohne, W., Hurles, M.E., Noegel, A.A., Baig, S.M., Nurnberg, P., and Jackson, A.P. 2014. Mutations in PLK4, encoding a master regulator of centriole biogenesis, cause microcephaly, growth failure and retinopathy. *Nat Genet* **46**(12): 1283-1292.

Minocherhomji, S., Ying, S., Bjerregaard, V.A., Bursomanno, S., Aleliunaite, A., Wu, W., Mankouri, H.W., Shen, H., Liu, Y., and Hickson, I.D. 2015. Replication stress activates DNA repair synthesis in mitosis. *Nature* **528**(7581): 286-290.

Murray, J.E., van der Burg, M., H, I.J., Carroll, P., Wu, Q., Ochi, T., Leitch, A., Miller, E.S., Kysela, B., Jawad, A., Bottani, A., Brancati, F., Cappa, M., Cormier-Daire, V., Deshpande, C., Faqeih, E.A., Graham, G.E., Ranza, E., Blundell, T.L., Jackson, A.P., Stewart, G.S., and Bicknell, L.S. 2015. Mutations in the NHEJ component XRCC4 cause primordial dwarfism. *Am J Hum Genet* **96**(3): 412-424.

Musio, A., Selicorni, A., Focarelli, M.L., Gervasini, C., Milani, D., Russo, S., Vezzoni, P., and Larizza, L. 2006. X-linked Cornelia de Lange syndrome owing to SMC1L1 mutations. *Nat Genet* **38**(5): 528-530.

Nicholas, A.K., Khurshid, M., Desir, J., Carvalho, O.P., Cox, J.J., Thornton, G., Kausar, R., Ansar, M., Ahmad, W., Verloes, A., Passemard, S., Misson, J.P., Lindsay, S., Gergely, F., Dobyns, W.B., Roberts, E., Abramowicz, M., and Woods, C.G. 2010. WDR62 is associated with the spindle pole and is mutated in human microcephaly. *Nat Genet* **42**(11): 1010-1014.

Nielsen, C.F., Huttner, D., Bizard, A.H., Hirano, S., Li, T.N., Palmai-Pallag, T., Bjerregaard, V.A., Liu, Y., Nigg, E.A., Wang, L.H., and Hickson, I.D. 2015. PICH promotes sister chromatid disjunction and co-operates with topoisomerase II in mitosis. *Nat Commun* **6**: 8962.

Nishide, K. and Hirano, T. 2014. Overlapping and non-overlapping functions of condensins I and II in neural stem cell divisions. *PLoS genetics* **10**(12): e1004847.

O'Driscoll, M., Ruiz-Perez, V.L., Woods, C.G., Jeggo, P.A., and Goodship, J.A. 2003. A splicing mutation affecting expression of ataxia-telangiectasia and Rad3-related protein (ATR) results in Seckel syndrome. *Nat Genet* **33**(4): 497-501.

Oliveira, R.A., Coelho, P.A., and Sunkel, C.E. 2005. The condensin I subunit Barren/CAP-H is essential for the structural integrity of centromeric heterochromatin during mitosis. *Mol Cell Biol* **25**(20): 8971-8984.

Ono, T., Fang, Y., Spector, D.L., and Hirano, T. 2004. Spatial and temporal regulation of Condensins I and II in mitotic chromosome assembly in human cells. *Mol Biol Cell* **15**(7): 3296-3308.

Ono, T., Losada, A., Hirano, M., Myers, M.P., Neuwald, A.F., and Hirano, T. 2003. Differential contributions of condensin I and condensin II to mitotic chromosome architecture in vertebrate cells. *Cell* **115**(1): 109-121.

Qvist, P., Huertas, P., Jimeno, S., Nyegaard, M., Hassan, M.J., Jackson, S.P., and Borglum, A.D. 2011. CtIP Mutations Cause Seckel and Jawad Syndromes. *PLoS Genet* **7**(10): e1002310.

Santaguida, S. and Amon, A. 2015. Short- and long-term effects of chromosome mis-segregation and aneuploidy. *Nat Rev Mol Cell Biol* **16**(8): 473-485.

Savvidou, E., Cobbe, N., Steffensen, S., Cotterill, S., and Heck, M.M. 2005. Drosophila CAP-D2 is required for condensin complex stability and resolution of sister chromatids. *Journal of cell science* **118**(Pt 11): 2529-2543.

Shintomi, K. and Hirano, T. 2011. The relative ratio of condensin I to II determines chromosome shapes. *Genes Dev* **25**(14): 1464-1469.

Siddiqui, N.U., Rusyniak, S., Hasenkampf, C.A., and Riggs, C.D. 2006. Disruption of the Arabidopsis SMC4 gene, AtCAP-C, compromises gametogenesis and embryogenesis. *Planta* **223**(5): 990-997.

Smith, E.D., Xu, Y., Tomson, B.N., Leung, C.G., Fujiwara, Y., Orkin, S.H., and Crispino, J.D. 2004. More than blood, a novel gene required for mammalian postimplantation development. *Mol Cell Biol* **24**(3): 1168-1173.

Strunnikov, A.V., Hogan, E., and Koshland, D. 1995. SMC2, a Saccharomyces cerevisiae gene essential for chromosome segregation and condensation, defines a subgroup within the SMC family. *Genes Dev* **9**(5): 587-599.

Thornton, G.K. and Woods, C.G. 2009. Primary microcephaly: do all roads lead to Rome? *Trends Genet* **25**(11): 501-510.

Tibelius, A., Marhold, J., Zentgraf, H., Heilig, C.E., Neitzel, H., Ducommun, B., Rauch, A., Ho, A.D., Bartek, J., and Kramer, A. 2009. Microcephalin and pericentrin regulate mitotic entry via centrosome-associated Chk1. *J Cell Biol* **185**(7): 1149-1157.

Trimborn, M., Schindler, D., Neitzel, H., and Hirano, T. 2006. Misregulated chromosome condensation in MCPH1 primary microcephaly is mediated by condensin II. *Cell Cycle* **5**(3): 322-326.

Verloes, A., Drunat, S., Gressens, P., and Passemard, S. 1993. Primary Autosomal Recessive Microcephalies and Seckel Syndrome Spectrum Disorders. in *GeneReviews(R)* (ed. R.A. Pagon, M.P. Adam, H.H. Ardinger, S.E. Wallace, A. Amemiya, L.J.H. Bean, T.D. Bird, C.R. Dolan, C.T. Fong, R.J.H. Smith, and K. Stephens), Seattle (WA).

Wang, J., Chang, Y.F., Hamilton, J.I., and Wilkinson, M.F. 2002. Nonsense-associated altered splicing: a frame-dependent response distinct from nonsense-mediated decay. *Mol Cell* **10**(4): 951-957.

Wood, J.L., Liang, Y., Li, K., and Chen, J. 2008. Microcephalin/MCPH1 associates with the Condensin II complex to function in homologous recombination repair. *J Biol Chem* **283**(43): 29586-29592.

Woods, C.G., Bond, J., and Enard, W. 2005. Autosomal recessive primary microcephaly (MCPH): a review of clinical, molecular, and evolutionary findings. *Am J Hum Genet* **76**(5): 717-728.

Wright, C.F., Fitzgerald, T.W., Jones, W.D., Clayton, S., McRae, J.F., van Kogelenberg, M., King, D.A., Ambridge, K., Barrett, D.M., Bayzetinova, T., Bevan, A.P., Bragin, E., Chatzimichali, E.A., Gribble, S., Jones, P., Krishnappa, N., Mason, L.E., Miller, R., Morley, K.I., Parthiban, V., Prigmore, E., Rajan, D., Sifrim, A., Swaminathan, G.J., Tivey, A.R., Middleton, A., Parker, M., Carter, N.P., Barrett, J.C., Hurles, M.E., FitzPatrick, D.R., and Firth, H.V. 2014. Genetic diagnosis of developmental disorders in the DDD study: a scalable analysis of genome-wide research data. *Lancet* **385**(9975): 1305-1314.

Yamashita, D., Shintomi, K., Ono, T., Gavvovidis, I., Schindler, D., Neitzel, H., Trimborn, M., and Hirano, T. 2011. MCPH1 regulates chromosome condensation and shaping as a composite modulator of condensin II. *J Cell Biol* **194**(6): 841-854.